N62-15297 N62-15297

48p

550779

NASA TN D-1362

NASA TN D-1362

TECHNICAL NOTE

D-1362

WIND-TUNNEL INVESTIGATION OF TAIL BUFFET AT SUBSONIC AND TRANSONIC SPEEDS EMPLOYING A DYNAMIC ELASTIC AIRCRAFT MODEL

By Robert N. Rigby and Elden S. Cornette

Langley Research Center
Langley Station, Hampton, Va.

NATIONAL AERONAUTICS AND SPACE ADMINISTRATION

WASHINGTON September 1962

1F

NATIONAL AERONAUTICS AND SPACE ADMINISTRATION

TECHNICAL NOTE D-1362

WIND-TUNNEL INVESTIGATION OF TAIL BUFFET AT SUBSONIC AND TRANSONIC SPEEDS EMPLOYING A DYNAMIC ELASTIC AIRCRAFT MODEL

By Robert N. Rigby and Elden S. Cornette

L
1
8
8
3

SUMMARY

Buffet tests were conducted with a complete model of a current supersonic attack aircraft at subsonic and transonic Mach numbers. The lifting surfaces and the aft-fuselage structure of the model were dynamically and elastically scaled. In addition to the basic configuration, the model was tested with wing frequencies reduced by adding wing-tip weights, with wing removed, and with two deflection angles of the horizontal tail. Root-mean-square bending-moment fluctuations were measured near the root of the wing, of the horizontal tail, and of the vertical tail. In addition, velocity fluctuations in the flow near the horizontal-tail location were measured by hot-wire probes which replaced the horizontal tail.

The flow fluctuations of the wing wake were at the horizontal-tail location only for negative angles of attack of the model. At positive angles, the flow fluctuations caused vertical-tail buffeting but not horizontal-tail buffeting. The intensity of the flow fluctuations was reduced by the addition of wing-tip weights; the vertical-tail response was also reduced. The flow fluctuations varied in intensity with position but did not exhibit any predominant frequency.

INTRODUCTION

Wing buffet has been studied in several experimental investigations, and some success has been achieved in predicting flight wing buffet loads from tunnel tests on simplified models. (See ref. 1.) However, only a limited amount of experimental data on tail buffet is available. Some of these data (ref. 2) indicate that tail buffet may be the response of the tail surfaces to three possible inputs: the separation of the flow over the tail surface, fluctuations in the flow impinging upon the tail surface (for example, fluctuations in the wing wake), and motion of other lifting surfaces transmitted through the fuselage structure.

In the present investigation, a complete model of a current supersonic attack aircraft was used to study these inputs to tail buffet. The model lifting surfaces and aft fuselage were dynamically and elastically scaled. The model was tested at subsonic and transonic Mach numbers over a range of stagnation pressures from 0.37 atmosphere to 0.74 atmosphere and over an angle-of-attack range. Root-mean-square bending-moment fluctuations near the root of the lifting surfaces were measured for the basic model configuration and for model configurations with wing frequencies reduced by adding wing-tip weights, with wings removed, and with the deflection angle of the horizontal tail varied. Also, the velocity fluctuations in the wing wake were measured with hot-wire probes (which replaced the horizontal tail).

L
1
8
8
3

SYMBOLS

$\bar{c}$ mean aerodynamic chord, ft

C_L lift coefficient, $\frac{\text{Lift}}{qS}$

g structural damping coefficient

h normalized deflection at points on elastic axis of lifting surfaces

m mass per unit length of exposed panel of lifting surface (along elastic axis), slug/ft

M free-stream Mach number

p_t free-stream total pressure, atm

q free-stream dynamic pressure, $\frac{\rho V^2}{2}$, lb/sq ft

S wing planform area, sq ft

V free-stream velocity, ft/sec

y nondimensional spanwise distance measured from fuselage center line, fraction of semispan

α angle of attack, deg

δ_H angle of horizontal tail relative to fuselage reference line, deg

η nondimensional distance measured along elastic axis of lifting surface from fuselage center line, fraction of elastic axis length

ρ free-stream density, slugs/cu ft

σ_B root-mean-square value of the bending-moment fluctuations (standard deviation from mean), in-lb

L 1 8 8 3

σ_F root-mean-square value of the velocity fluctuations (standard deviation from mean), ft/sec

Subscripts:

W wing

H horizontal tail

V vertical tail

TUNNEL

The investigation was conducted in the Langley 8-foot transonic pressure tunnel. This tunnel has a rectangular test section with the upper and lower walls slotted longitudinally to allow continuous operation through the transonic speed range with negligible effects of choking and blockage. The free-stream stagnation pressure can be varied from 1/4 to 2 atmospheres.

The local Mach number distribution throughout the test-section region occupied by the model was reasonably uniform with a maximum deviation from the average free-stream Mach number of 0.003 at the highest Mach number tested. Changes in free-stream stagnation pressure have essentially no effect on the Mach number distribution.

MODEL

General Description

A complete model of a current supersonic attack aircraft was used in this investigation. A three-view drawing of the model is presented

in figure 1 along with the geometrical characteristics of the lifting surfaces. The model had a wide fuselage, shoulder-mounted sweptback wing, sweptback vertical tail, and sweptback all-movable horizontal tail. The model was geometrically similar to the full-scale aircraft with two exceptions: the engine air inlets were faired closed, and external aluminum doublers were added to the root sections of the wing and horizontal tail. One-eighth-inch-wide boundary-layer transition strips of number 60 carborundum grains were placed at the 10-percent chord of the lifting surfaces and at fuselage stations located at 10 percent of the length measured from the nose. The lifting surfaces and the aft-fuselage structure were dynamically and elastically scaled to those of the full-scale aircraft.

L
1
8
8
3

Construction

The model fuselage consisted of a rigid forward section and a flexible aft section. (See fig. 2.) The forward-fuselage section contained a six-component balance and the attachment structure for the wing. The aft-fuselage section was an aluminum-alloy tube cantilevered from the forward-fuselage section and had a built-up structure to support the horizontal and vertical tails. The aerodynamic shape of the fuselage was provided by a relatively thin plastic shell attached to each fuselage section. The fuselage was attached to the tunnel support system by passing the tunnel sting through the aft-fuselage tube to the six-component balance. Adequate clearance between the aft-fuselage tube and the tunnel sting was allowed.

The wings were constructed around a single aluminum-alloy spar bonded to a magnesium root rib. (See fig. 2.) Foamed plastic at the leading and trailing edge of the spar provided the airfoil shape. A thin aluminum skin was bonded to the spar and the foamed plastic to provide strength and stiffness. Thin aluminum-alloy doublers were added externally to the wing root region on the upper and lower surfaces for additional strength. These external doublers increased the thickness by as much as 0.10 inch and increased the maximum thickness at the wing root region from 5.0- to 5.7-percent chord. Lead weights were imbedded in the foamed plastic to provide the required mass distribution. Each wing was mounted to the forward-fuselage section with two pin joints. The two wings were joined by a stainless-steel splice plate which was attached to the wing root ribs. For some tests, strips of 0.08-inch-thick lead tape were fastened externally to the upper and lower surfaces of the wing tips to reduce the wing frequencies.

The vertical- and horizontal-tail surfaces were constructed in a manner similar to the wing construction (fig. 2), that is, with a metal spar and root rib, foamed plastic filler, and a thin aluminum skin. A stainless-steel splice plate was attached to the root rib of each tail

surface and was cantilever-mounted from the aft-fuselage tube. The horizontal tail had thin aluminum-alloy doublers with maximum thickness of 0.10 inch which increased the maximum thickness at the root region of the horizontal tail from 5.0- to 5.9-percent chord.

Physical Properties

The natural vibration frequencies of the model mounted on the tunnel sting support system were determined by exciting the model with an electrodynamic shaker. The resulting natural frequencies are presented in table I, and a sketch of the corresponding node lines on the lifting surfaces is presented in figure 3. No vibration mode consisting primarily of aft-fuselage motion could be excited. The lead weights added to the wing tips reduced the first symmetrical wing-bending frequencies by 18 percent and also reduced the other measured wing frequencies but had essentially no effect upon the measured frequencies of the tail surfaces.

L
1
8
8
3

The structural damping coefficient g was obtained for some vibration modes by suddenly removing the excitation and measuring the decay rate of the motion. Decay rates were measured for several initial amplitudes, and an average value of g was obtained. (See table I.)

The bending mode shapes (fig. 4) for the basic wing and the horizontal tail were determined by the "1 g method" described in reference 3 and by an optical method. The mode shapes for the weighted wing and the vertical tail were not measured.

The mass distribution properties of the exposed panel of the lifting surfaces (fig. 5) were calculated from the distribution of the construction materials. These calculations do not include the wing-tip weights which were 0.00171 slug and 0.00164 slug for the right and left wing, respectively. Although the tip weights differed between the wings, the resulting frequencies were essentially the same.

The torsional stiffness GJ of the aft-fuselage tube varied linearly with position from 8.34×10^6 lb-in.^{2} at the forward end to 4.56×10^6 lb-in.^{2} at the rearward end. The bending stiffness EI of the aft-fuselage tube varied similarly from 2.40×10^6 lb-in.^{2} to 1.58×10^6 lb-in.^{2}.

Instrumentation

A conventional internally mounted six-component strain-gage balance measured the static aerodynamic forces and moments acting upon the model. The angle of attack was measured by an electrical strain-gage pendulum-type inclinometer mounted in the forward-fuselage section. A static orifice at the rearward end of the model measured the model base pressure.

Strain gages were mounted near the root of the lifting surfaces to measure the bending-moment fluctuations and the location and orientation of the effective bending-moment axes are presented in figure 6.

With the horizontal tail removed, two hot-wire probes were mounted from the aft-fuselage tube (fig. 7) to measure the flow fluctuations at the location of the left horizontal tail. The hot-wire probes had single hot wires oriented along the spanwise direction which were sensitive primarily to the velocity fluctuations in the chordwise direction. The hot wires were 0.0005-inch-diameter platinum wire and had a length of 0.125 inch. The position of the hot-wire probes is shown in figure 8. One hot-wire probe was fixed near the aft fuselage. The other hot-wire probe was located at three vertical chordwise positions (at the axis of rotation of the horizontal tail, 3.92 inches forward of the axis of rotation, and 3.92 inches forward and 0.41 inch above the axis of rotation) and at four spanwise positions for each vertical-chordwise position (0.58, 0.72, 0.86, and 1.00 fraction of horizontal-tail semispan). L 1 8 8 3

The steady-state part of each strain gage or hot-wire signal was eliminated electrically. The remaining fluctuating signals were recorded on magnetic tape with a 45-second data sample length. The mean-square values of selected signals were visually recorded during testing from a thermocouple meter. A low-frequency oscillator and a root-mean-square voltmeter were used to supply a known calibration signal.

TESTS

The tunnel tests were divided into three series. In the first and second series, only bending-moment fluctuations near the root of the lifting surfaces were measured. In the third series, velocity fluctuations at the location of the horizontal tail were also measured. The model configurations and the angle-of-attack range for each test series are presented in table II; the Mach number and tunnel stagnation pressure range for each test series are presented in figure 9. For all tests, automatic tunnel air temperature controls maintained a uniform stagnation temperature of approximately 120° F. The dewpoint of the tunnel air was maintained near 0° F.

REDUCTION OF DATA

The data from the bending gages and the hot-wire probes were reduced from magnetic tape records to the form of root-mean-square values of bending-moment and velocity fluctuations and to the form of power-spectral-density plots. The root-mean-square values were obtained

from an average of the output of the mean-square vacuum-tube voltmeters over the 45-second data sample length. The output of these voltmeters oscillated within a range of ±10 percent of the average value for most of the data points. The power-spectral-density plots were obtained for some data points through the use of analog equipment described in reference 4. Thirty-second samples from the 45-second data records were analyzed. The effective band width of the scanning band-pass filter used in the analog equipment was approximately 8 cycles per second for the bending gage signals and approximately 6 cycles per second for the hot-wire probe signals.

L
1
8
8
3

RESULTS AND DISCUSSION

General Discussion

The lift characteristics of the basic model with $\delta_H = 0^\circ$ and $\delta_H = -6^\circ$ are presented in figure 10. The buffet characteristics are presented in figures 11 to 24. The intensity of the fluctuation in the bending moment at the root of the wing, of the vertical tail, and of the horizontal tail as well as the intensity of the velocity fluctuations at the horizontal-tail location are indicated by the root-mean-square values σ_B and σ_F. These data are presented as a function of angle of attack rather than of lift coefficient in order to facilitate comparison between model configurations with wing or horizontal tail removed. The root-mean-square values contain extraneous contributions caused by instrumentation noise, tunnel turbulence, and sting support motion. For these tests, it is believed that the magnitude of the first two contributions is indicated by the root-mean-square values at $\alpha = 0^\circ$. A detailed view of the frequency content of the fluctuating signals is provided by the power-spectral-density plots.

Wing Buffet

At low-to-moderate subsonic Mach numbers, the root-mean-square bending-moment fluctuations for the wing $\sigma_{B,W}$, generally increase with increasing angle of attack α. (See figs. 11 and 12.) Also, the buffet characteristics of the wing at negative α were similar to those at positive α for subsonic Mach numbers. (See fig. 12.) Unusually severe wing buffeting occurred near $\alpha = 8^\circ$ for $M = 0.90$, $p_t = 0.599$ atmosphere, and near $\alpha = 9^\circ$ for $M = 0.95$, $p_t = 0.371$ atmosphere. (See fig. 11.) This phenomenon has occurred previously at similar test conditions in a buffet investigation with sweptback wings, and several possible causes have been discussed in reference 5. The cause of the phenomenon for this investigation has

not been determined. At Mach number 1.0, severe buffeting did not occur, and the increase of $\sigma_{B,W}$ with α was comparatively small. This latter result is consistent with other buffet investigations of sweptback wings at transonic Mach numbers. (See ref. 6.)

At the higher Mach numbers, changes in tunnel stagnation pressure yielded some significant variation in $\sigma_{B,W}$, but the range of p_t is not sufficiently large to study this effect in detail.

Reducing the wing first symmetrical bending frequency approximately 18 percent by adding wing-tip weights did not significantly change the wing buffet characteristics. (See fig. 12.) Further, wing buffet characteristics were not appreciably affected by the deflection angle of the horizontal tail nor by the replacement of the horizontal tail with the hot-wire probes. Therefore, data for the latter two configurations are not presented.

L
1
8
8
3

Typical power-spectral-density plots of the wing bending-moment fluctuations during buffeting are presented in figure 13. As expected, the main portion of the power was centered near the frequency corresponding to the first symmetric bending modes. (See table I.) The peak at this frequency was usually larger for the weighted wing than for the basic wing, although the $\sigma_{B,W}$ values were approximately the same. (See fig. 12(b).) A much smaller amount of power was noticeable near the first antisymmetric wing-bending frequencies. Also, a small amount of power was centered at approximately 40 cycles per second, which corresponds to a rigid-body pitching mode.

Flow Characteristics at Horizontal-Tail Location

The flow characteristics near the horizontal-tail location at the lower subsonic Mach numbers were measured with hot-wire probes (the horizontal tail being removed) which were sensitive to velocity fluctuations primarily in the chordwise direction. The root-mean-square values of the velocity fluctuations σ_F are presented in figure 14 as a function of α. The σ_F values were essentially constant for positive α; however, for α less than approximately -5°, the σ_F values increased appreciably with decreasing α. These results indicate that the flow fluctuations in the wake of the wing were in the vicinity of the horizontal tail only at negative α, and that at positive α the wing-wake flow fluctuations probably passed above the vicinity of the horizontal tail.

Addition of the external wing-tip weights generally reduced the σ_F values at negative angles of attack of the model. (See fig. 14.)

Similar results were obtained from measurements of the bending-moment fluctuations of the vertical tail. It is unlikely that the aerodynamic interference of the wing-tip weights caused the reduction of the σ_F values, since the presence of the external additions on the wing would be expected to increase the intensity of the flow fluctuations. It appears, rather, that the wing-tip weights altered the motion of the wing and that this alteration reduced the wing-wake flow fluctuations. The σ_F values obtained with the wings removed were approximately the same as corresponding values with the wing on at positive angle of attack of the model. The wing-off data are, therefore, not presented.

L
1
8
8
3

The σ_F values varied considerably with the position of the hot-wire probe as is shown in figure 15 which is a crossplot of the data in figure 14. In the spanwise direction, the σ_F values varied from the smallest values near the fuselage to larger values near the tip of the horizontal tail, the largest σ_F values usually being near 0.84 span. The limited number of tests do not permit an examination of the variation of σ_F in the chordwise and vertical directions except to state that such changes in probe location lead to appreciable changes in σ_F. (See figs. 14 and 15.)

Power-spectral-density plots of the velocity fluctuations in the wake of the wing are presented in figure 16. The main portion of the power was confined to the lower frequencies. For $M = 0.33$ and $M = 0.56$ (figs. 16(a) and 16(b)), the power spectral density decreased with increasing frequency with no predominant peaks (excluding electrical noise at 60 cps and 120 cps). For $M = 0.74$, a broad peak occurred near 250 cycles per second (fig. 16(c)) with a gradual decrease in power with increasing frequency above 250 cycles per second. The shape of the power-spectral-density plots for the wakes of the basic wing and the wing with added mass were similar although the power level was usually larger for the basic wing. Thus, the addition of mass to the wing affected the wing-wake flow fluctuations only in overall intensity and not in the frequency content.

Horizontal-Tail Buffet

The effect of model angle of attack on the root-mean-square bending-moment fluctuations for the horizontal tail $\sigma_{B,H}$ for $\delta_H = -6^\circ$ are presented in figure 17. For all Mach numbers below 1.0, $\sigma_{B,H}$ is shown to increase with increasing α above approximately 9° or 10°. Values of horizontal-tail response for the horizontal tail at $\delta_H = 0^\circ$ and $\delta_H = -6^\circ$ are compared with corresponding values of the wing response in figure 18. This figure includes wing buffet data only for $\delta_H = 0^\circ$ since the wing response has previously been indicated to be essentially independent of δ_H. For positive angles of attack of the model, the

bending-moment response of the wing (fig. 18) rises at lower α than the corresponding values for the horizontal tail. These results indicate that, for positive α, buffeting of the horizontal tail was not caused by the wing-wake flow fluctuations but rather was caused by separation of the flow over the horizontal tail. This conclusion is substantiated by the results of the measurements of the velocity fluctuations in the flow near the location of the horizontal tail (fig. 14) for positive angles of attack of the model. These flow measurements indicated no flow disturbances in the vicinity of the horizontal tail at positive angles of attack of the model. At negative angles of attack, the limited amount of data shows that the horizontal-tail response (fig. 18) increases at approximately the same α at which the wing response increases. This result indicates that the wing-wake flow fluctuations may have affected the horizontal-tail buffeting at negative α. This premise is again supported by the measurements of the flow fluctuations. (See fig. 14.)

L
1
8
8
3

Since the wing-wake flow fluctuations were not near the location of the horizontal tail at positive angles of attack of the model, the addition of mass to the wing did not significantly affect the horizontal-tail response for positive α. (See fig. 19.)

The results of these tests differ considerably from those of reference 2 which indicated a considerable effect of the wing wake on horizontal-tail buffeting. This difference is probably due to different tail locations. In the tests of reference 2, the horizontal tail was above the plane of the wing, whereas, in the present tests, the horizontal tail was below the wing plane.

The power spectral density of the horizontal-tail response (fig. 20) indicates that the largest amount of power was centered near 200 cycles per second corresponding to the first symmetric bending mode of the horizontal tail. A significant amount of power appeared near 275 cycles per second, corresponding to the first antisymmetric bending mode of the horizontal tail. A small amount of power was usually centered near 140 cycles per second corresponding to a rigid-body pitch-translational mode. (See table I.) The lack of appreciable power at 80 cycles per second to 100 cycles per second indicates that the motion of the wing and vertical tail were not noticeably transmitted through the fuselage structure to the horizontal tail.

Vertical-Tail Buffet

At the lower Mach numbers, the root-mean-square bending-moment fluctuations of the vertical tail $\sigma_{B,V}$ increased with increasing angle of attack (fig. 21) in a manner similar to that of the wing buffet characteristics. (See fig. 11.) However, with the wing removed,

the $\sigma_{B,V}$ values remained small and essentially independent of α. (See fig. 22.) Since structural coupling between the wing and vertical tail was minimized by the model construction, these results indicate that the main contribution to vertical-tail buffeting was from flow fluctuations in the wake of the wing. Adding mass to the wing reduced the $\sigma_{B,V}$ values as shown in figure 22.

The effect of the horizontal tail on vertical-tail buffeting is indicated in figure 23 which compares the vertical-tail $\sigma_{B,V}$ values for three horizontal-tail configurations. The $\sigma_{B,V}$ values varied significantly between these three model configurations. It appears that the deflection angle of the horizontal tail affects the position of the wing wake and hence affects the flow fluctuations in the vicinity of the vertical tail.

L
1
8
8
3

The power spectral density of the vertical-tail response (fig. 24) shows the largest amount of power at approximately 88 cycles per second, corresponding to the first bending mode of the vertical tail. (See table I.) Another peak usually occurred at approximately 107 cycles per second. The only measured model frequency near this peak was the first antisymmetric bending of the basic wing. However, since the frequency of this peak remained the same for the configuration with wing frequencies reduced, this peak does not appear to correspond to a wing bending mode. Rather, this peak is thought to indicate response in a rigid-body yaw mode not discovered during the model vibration tests. The vertical-tail response did not show appreciable power at frequencies corresponding to the first bending modes of the horizontal tail but did contain small amounts of power at 140 cycles per second corresponding to rigid-body pitch-translation mode.

CONCLUSIONS

Buffet tests with a complete aircraft model have been conducted in the Langley 8-foot transonic pressure tunnel. The results of these tests indicate the following conclusions:

1. With the horizontal tails removed, wing-wake flow fluctuations were in the vicinity of the horizontal tail only at negative angles of attack of the model; at positive angles, the wing wake appeared to pass above the horizontal-tail location. Therefore, horizontal-tail buffeting at positive angles of attack was not caused by the wing wake but was primarily due to separation of the flow over the horizontal tail.

2. The intensity of the velocity fluctuations in the flow near the horizontal-tail location varied considerably with position and was generally reduced by addition of weights to the wing tip.

3. Vertical-tail buffeting appeared to be caused by the wing wake. Addition of weights to the wing tip reduced the vertical-tail response.

4. The velocity fluctuations in the wake of the wing did not exhibit any predominant frequency corresponding to wing vibration modes.

Langley Research Center,
National Aeronautics and Space Administration,
Langley Station, Hampton, Va., April 10, 1962.

L
1
8
8
3

REFERENCES

1. Davis, Don D., Jr., and Huston, Wilber B.: The Use of Wind Tunnels to Predict Flight Buffet Loads. NACA RM L57D25, 1957.

2. Rainey, A. Gerald, and Igoe, William B: Measurements of the Buffeting Loads on the Wing and Horizontal Tail of a 1/4-Scale Model of the X-1E Airplane. NACA RM L58F25, 1958.

3. Hanson, Perry W., and Tuovila, W. J.: Experimentally Determined Natural Vibration Modes of Some Cantilever-Wing Flutter Models by Using an Acceleration Method. NACA TN 4010, 1957.

4. Smith, Francis B.: Analog Equipment for Processing Randomly Fluctuating Data. Aero. Eng. Rev., vol. 14, no. 5, May 1955, pp. 113-119.

5. Cornette, Elden S.: Wind-Tunnel Investigation of the Effects of Wing Bodies, Fences, Flaps, and a Fuselage Addition on the Wing Buffet Response of a Transonic-Transport Model. NASA TN D-637, 1961.

6. Cornette, Elden S.: Wind-Tunnel Investigation of the Wing Buffet Response of a Variable-Wing-Sweep Model at Subsonic and Transonic Speeds. NASA TM X-443, 1961.

L
1
8
8
3

TABLE I.- VIBRATION FREQUENCIES AND STRUCTURAL DAMPING COEFFICIENTS

Vibration mode	Frequency, cps	g
Basic wing:		
First symmetric bending	78.8	0.014
First antisymmetric bending	97.0	0.014
Second symmetric bending	221.6	0.023
First symmetric torsion	355.8	0.007
Weighted wing:		
First symmetric bending	64.4	-----
First antisymmetric bending	83.7	-----
Second symmetric bending	201.0	-----
First symmetric torsion	321.7	-----
Horizontal tail:		
First symmetric bending	196.9	0.023
First antisymmetric bending	270.6	0.024
Second symmetric bending	565.9	-----
First symmetric torsion	454.2	-----
Vertical tail:		
First bending	79.0	0.022
Second bending	350.5	0.026
First torsion	435.5	-----
Rigid body:		
First coupled pitch-vertical translation	7.2	-----
Second coupled pitch-vertical translation	29.3	-----
Roll	35.8	-----
Pitch	38.0	-----
Third coupled pitch-vertical translation	146.6	-----

L
1
8
8
3

TABLE II.- DESCRIPTION OF MODEL CONFIGURATIONS FOR EACH TEST SERIES

Test series	Configuration		Angle of attack of model, deg	Angle of deflection of horizontal tail, deg
	Wing	Horizontal tail		
I	Basic	Basic	0 to 18 or to wing load limit	-6
II	Basic, weighted, removed	Basic	-9 to 15	0
III	Basic, weighted, removed	Replaced by hot wires	-9 to 15	--

Geometrical characteristics of model

Wing:	
Airfoil section	Mod. NACA 65A005
Area, sq ft	3.43
Aspect ratio	4.0
Taper ratio	0.20
Sweepback of quarter-chord line, deg	37.5
Horizontal tail:	
Airfoil section	65A005
Exposed area, sq ft	0.86
Aspect ratio (exposed area)	2.5
Taper ratio (exposed area)	0.20
Sweepback of quarter-chord line, deg	45
Vertical tail:	
Airfoil section	65A005
Exposed area, sq ft	0.49
Aspect ratio (exposed area)	1.5
Taper ratio (exposed area)	0.35
Sweepback of quarter-chord line, deg	45

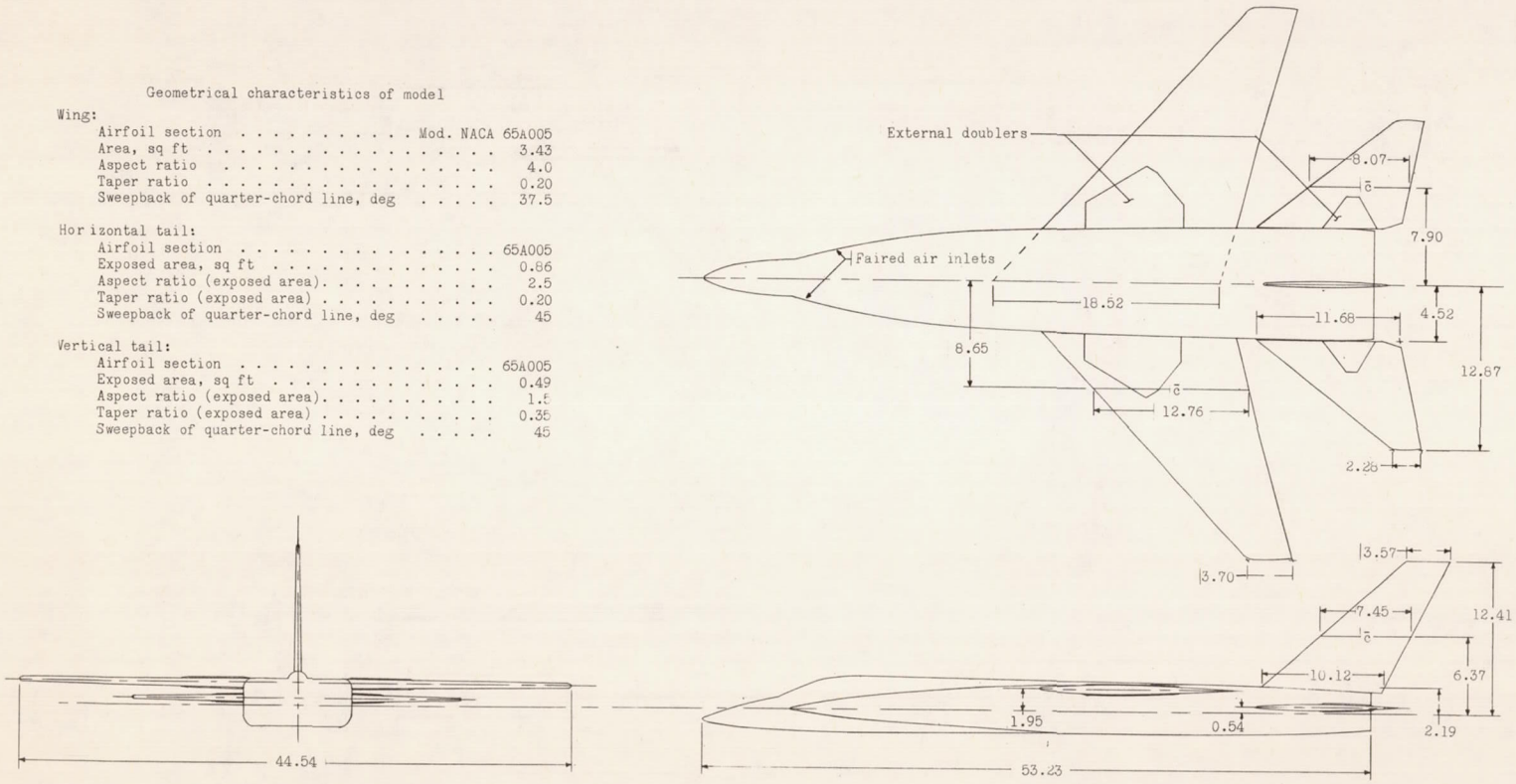

Figure 1.- Drawing of model. All linear dimensions are in inches.

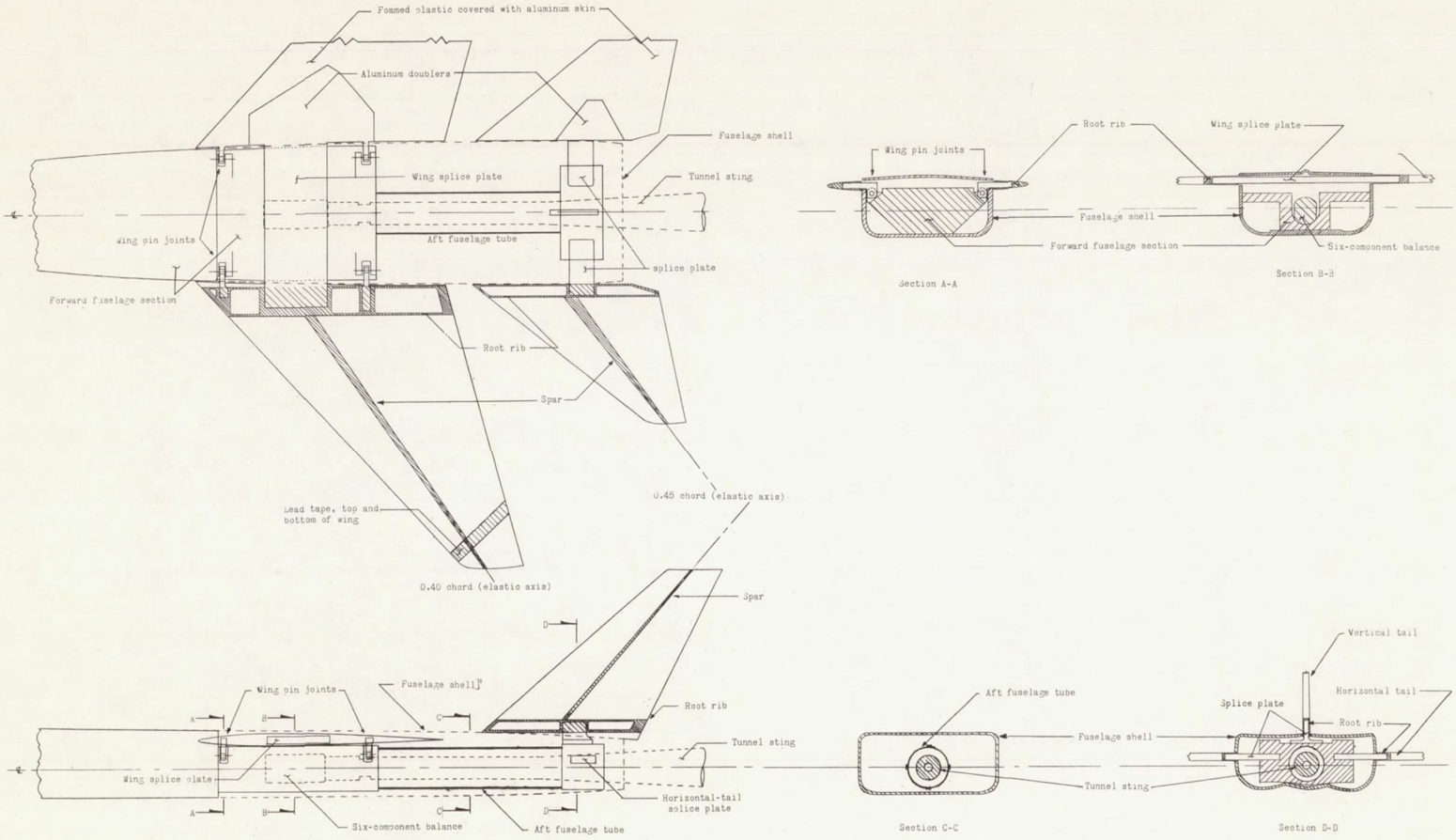

Figure 2.- Simplified sketch of model construction.

L-1883

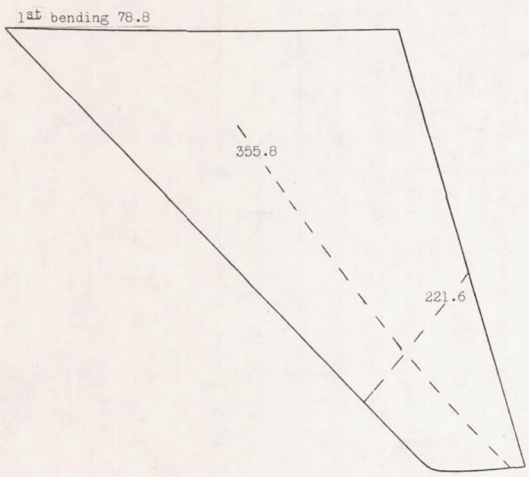

(a) Basic wing, symmetric modes.

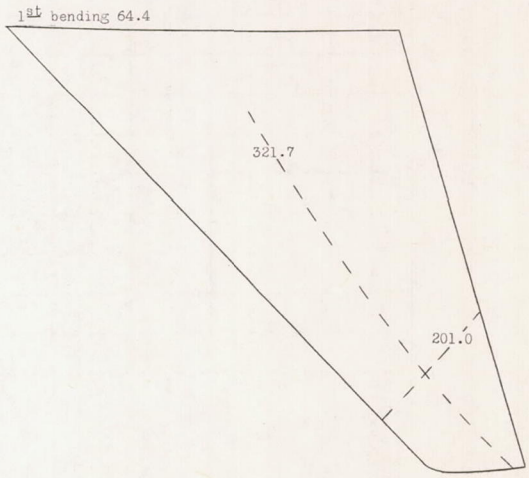

(b) Weighted wing, symmetric modes.

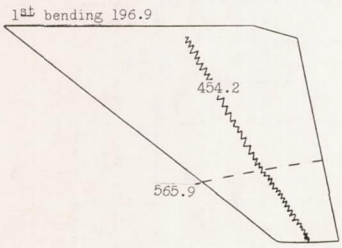

(c) Horizontal tail, symmetric modes.

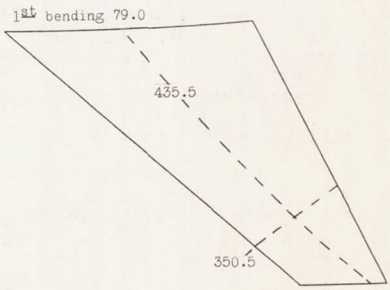

(d) Vertical tail.

Figure 3.- Node lines on lifting surfaces for model mounted on sting support system. All frequencies are in cycles per second.

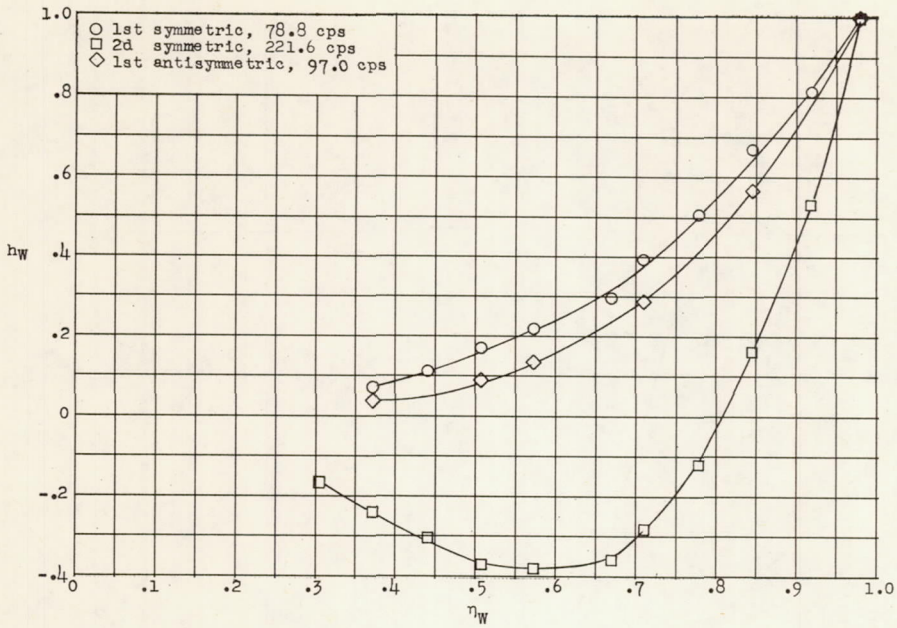

(a) Basic wing.

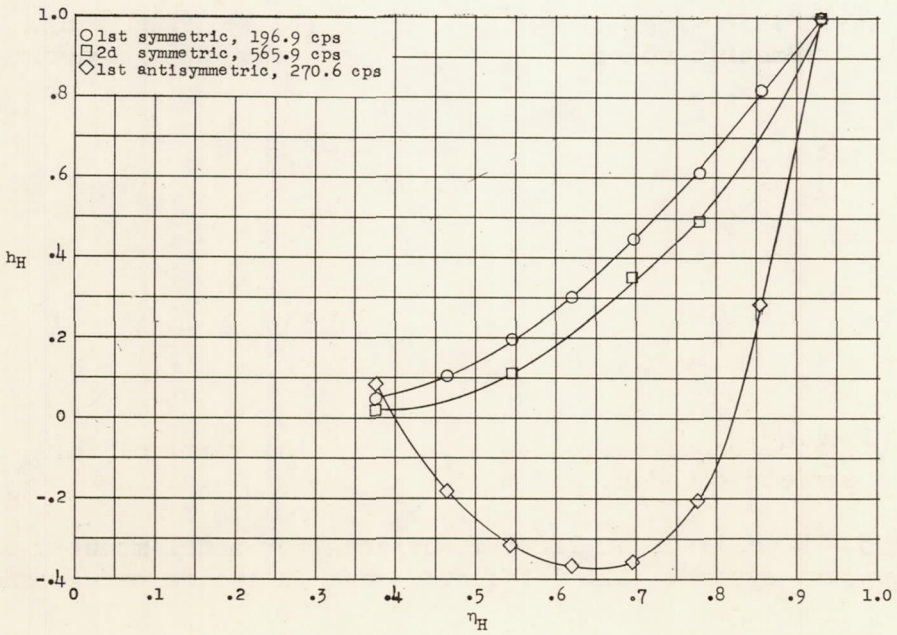

(b) Horizontal tail.

Figure 4.- Nondimensionalized bending-mode shapes for basic wing and horizontal tail.

L-1883

L-1883

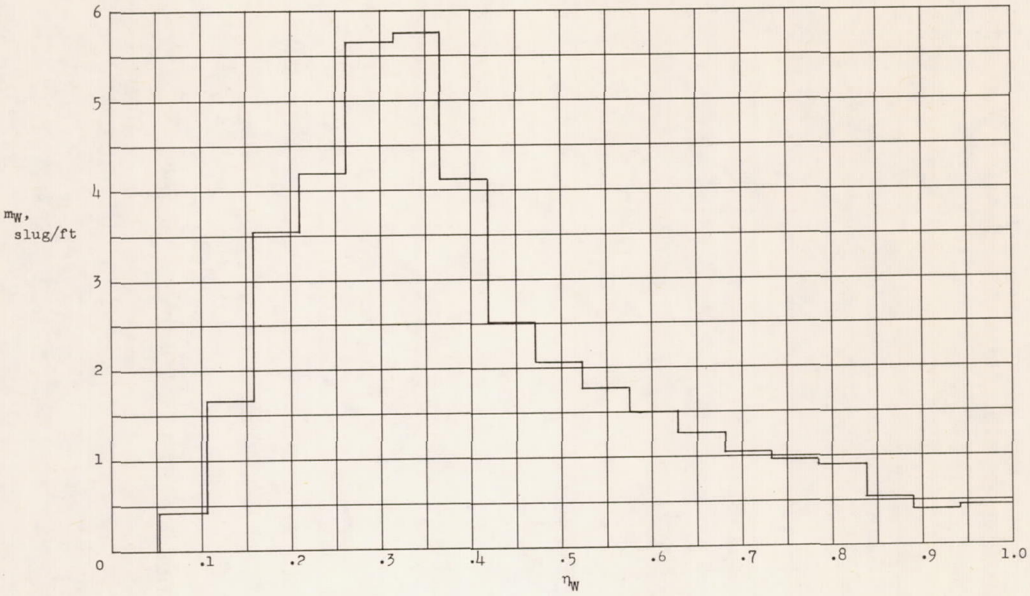

(a) Basic wing.

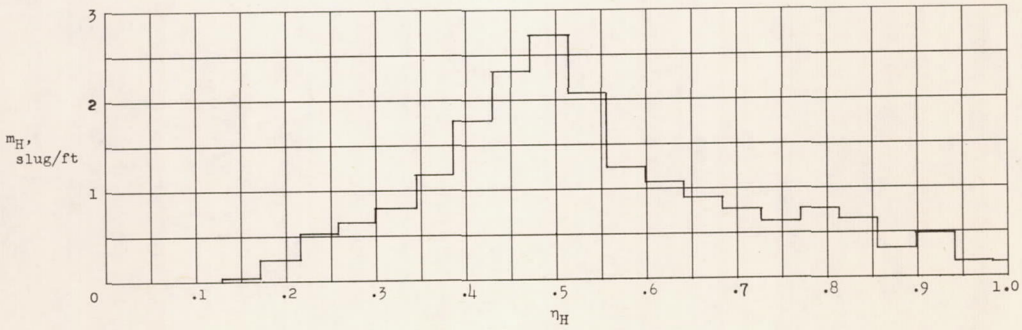

(b) Horizontal tail.

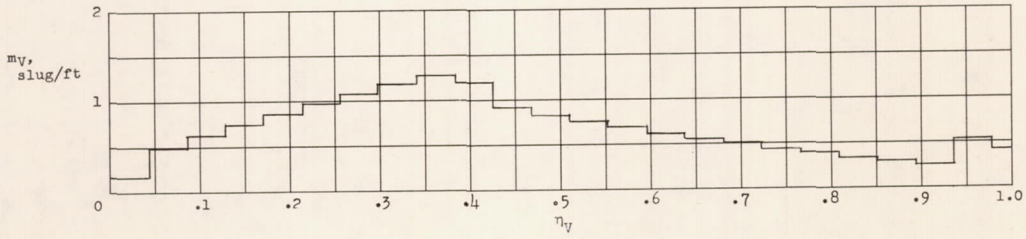

(c) Vertical tail.

Figure 5.- Mass distribution of exposed panel of lifting surfaces.

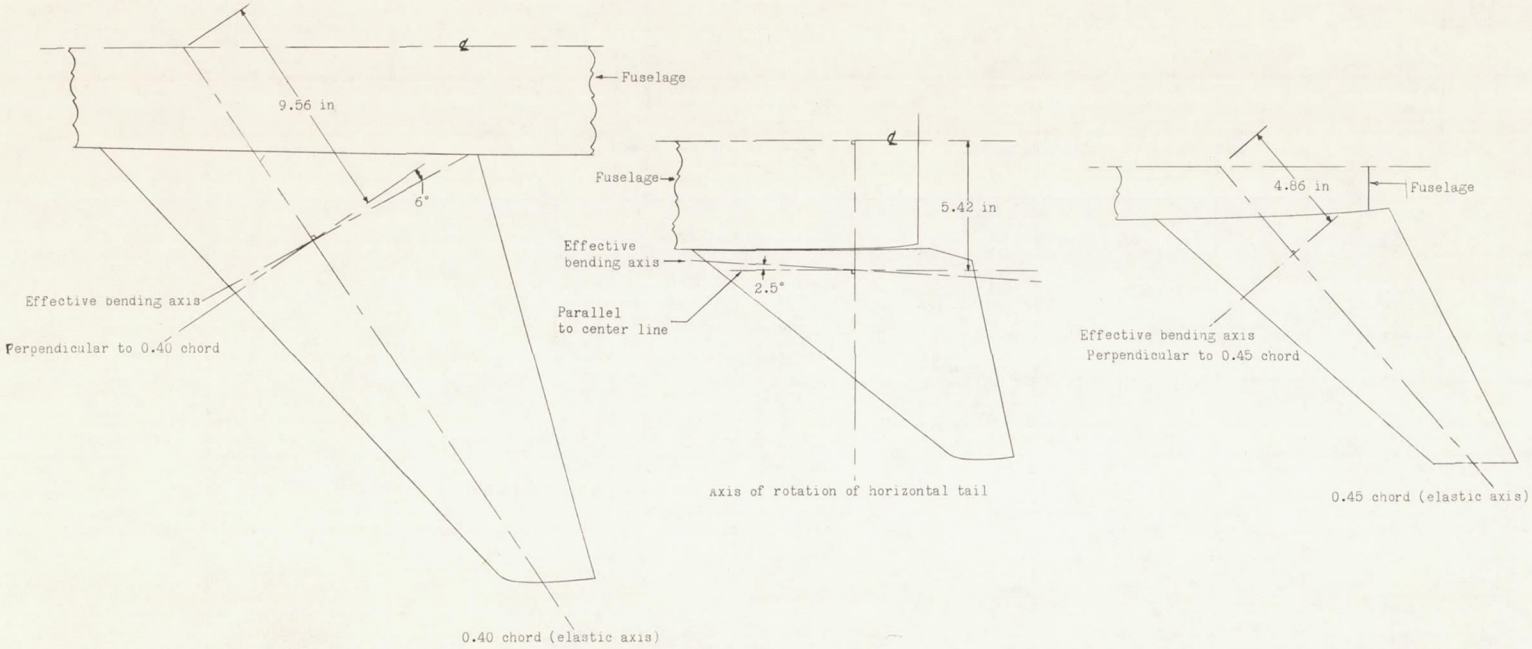

(a) Wing. (b) Horizontal tail. (c) Vertical tail.

Figure 6.- Location and orientation of effective bending axes of strain gages.

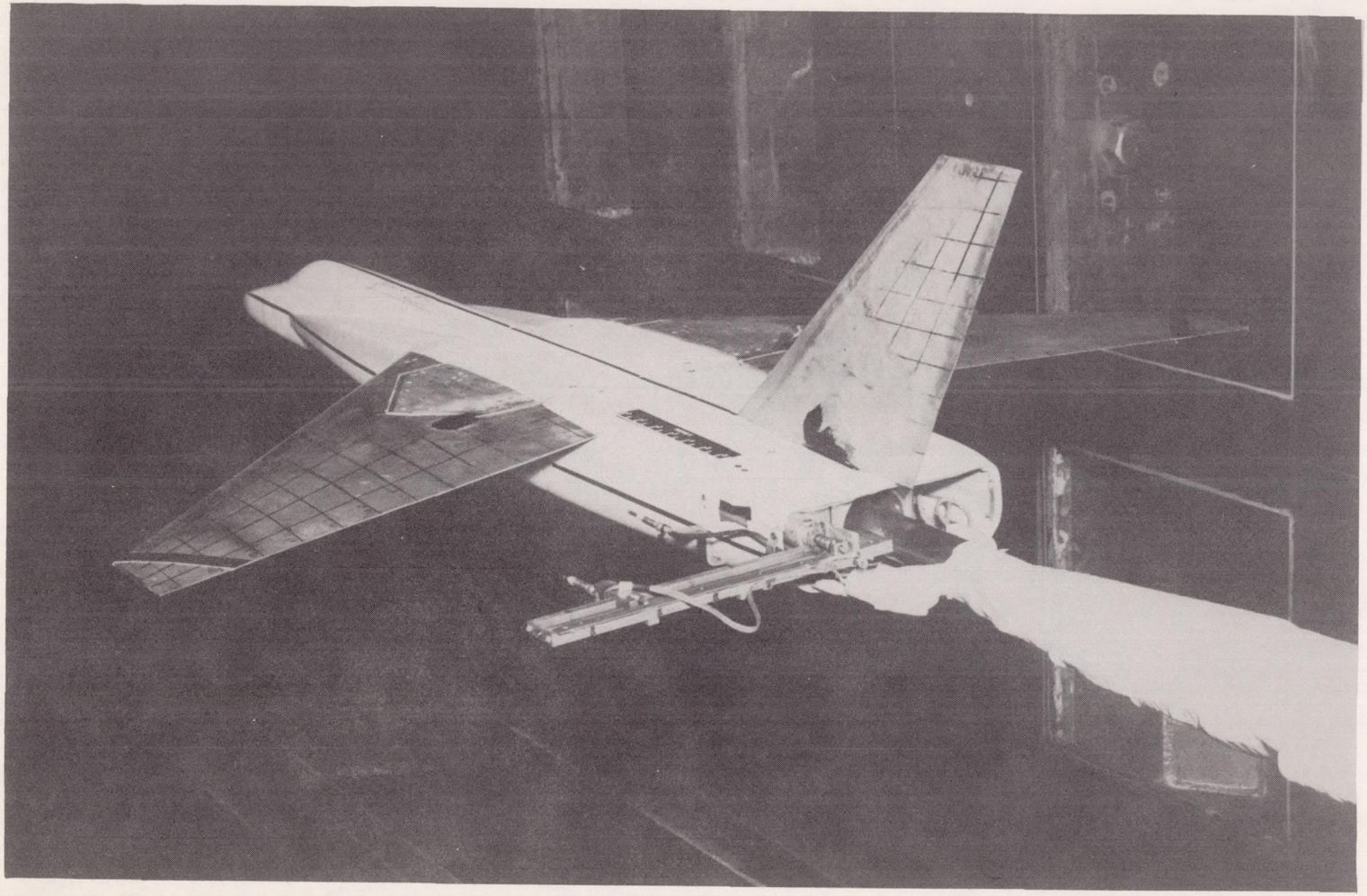

L-60-4413

Figure 7.- Photograph of model in tunnel with hot-wire probes replacing horizontal tail. Weighted wing.

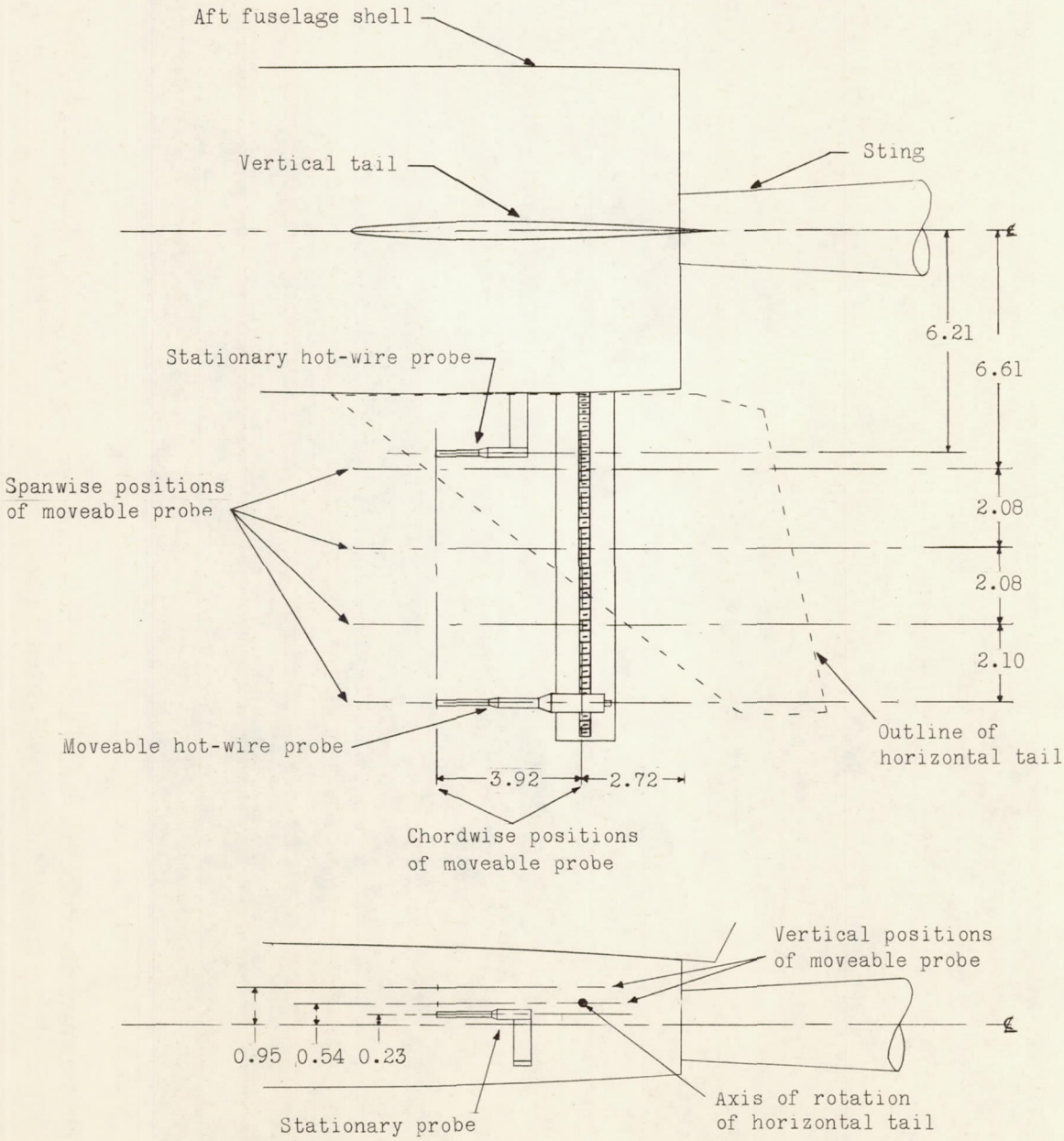

Figure 8.- Positions of hot-wire probes. Outline of horizontal tail included although horizontal tail removed for hot-wire tests. All linear dimensions are in inches.

L-1883

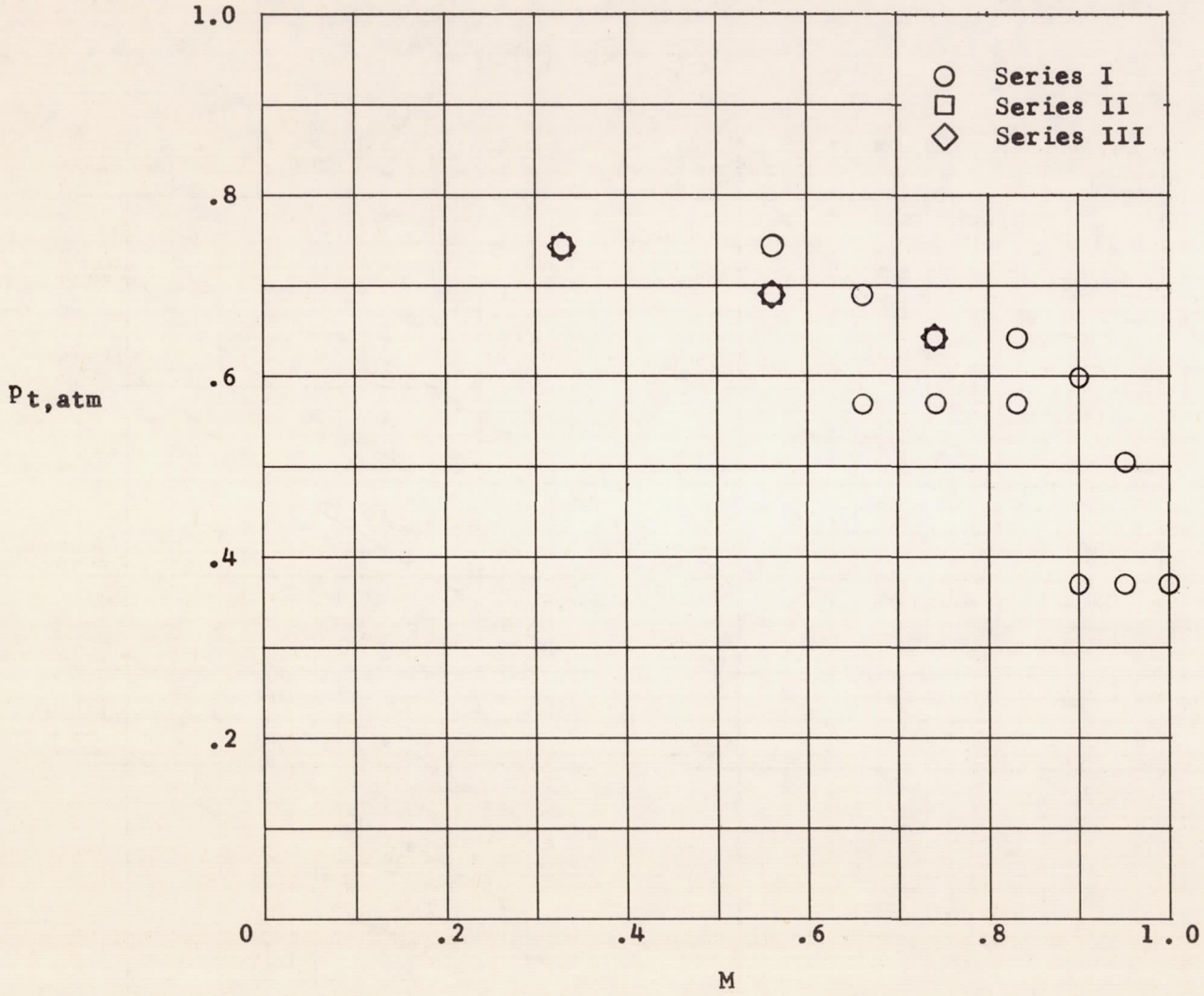

Figure 9.- Mach numbers and tunnel stagnation pressures for each test series.

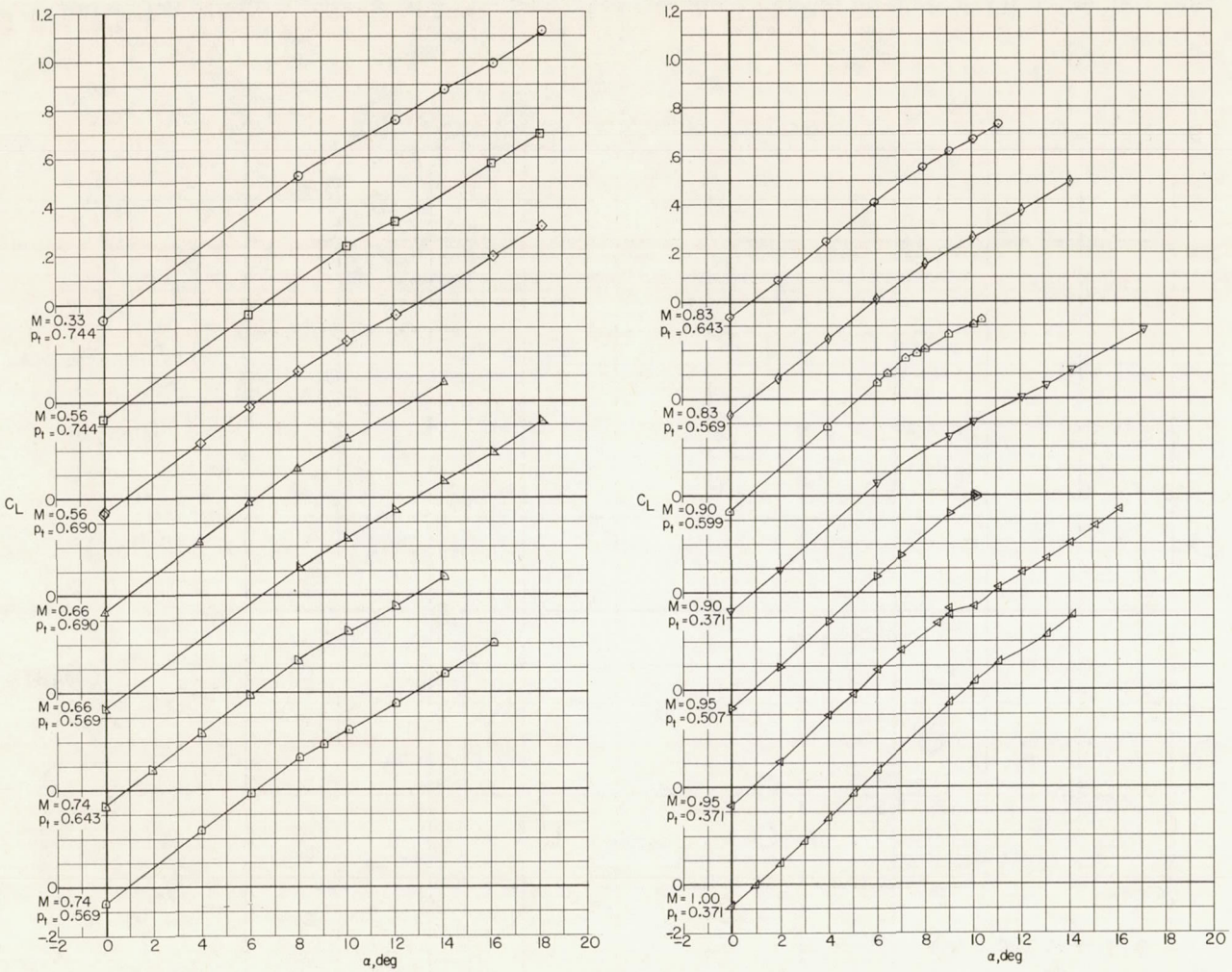

(a) $\delta_H = -6^\circ$.

Figure 10.- Lift characteristics of the model with basic wing. (p_t is measured in atmospheres.)

L-1883

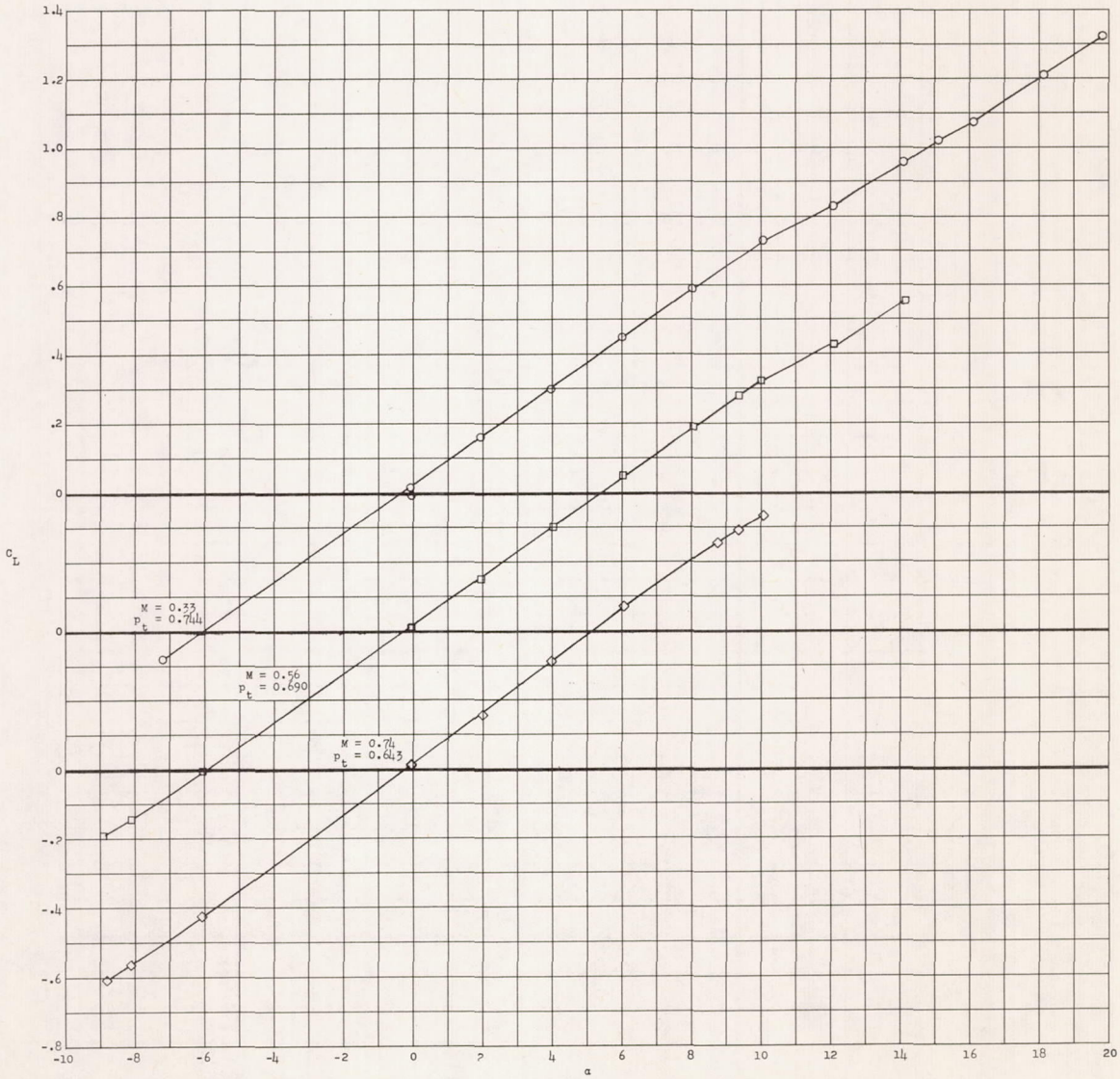

(b) $\delta_H = 0^{\circ}$.

Figure 10.- Concluded.

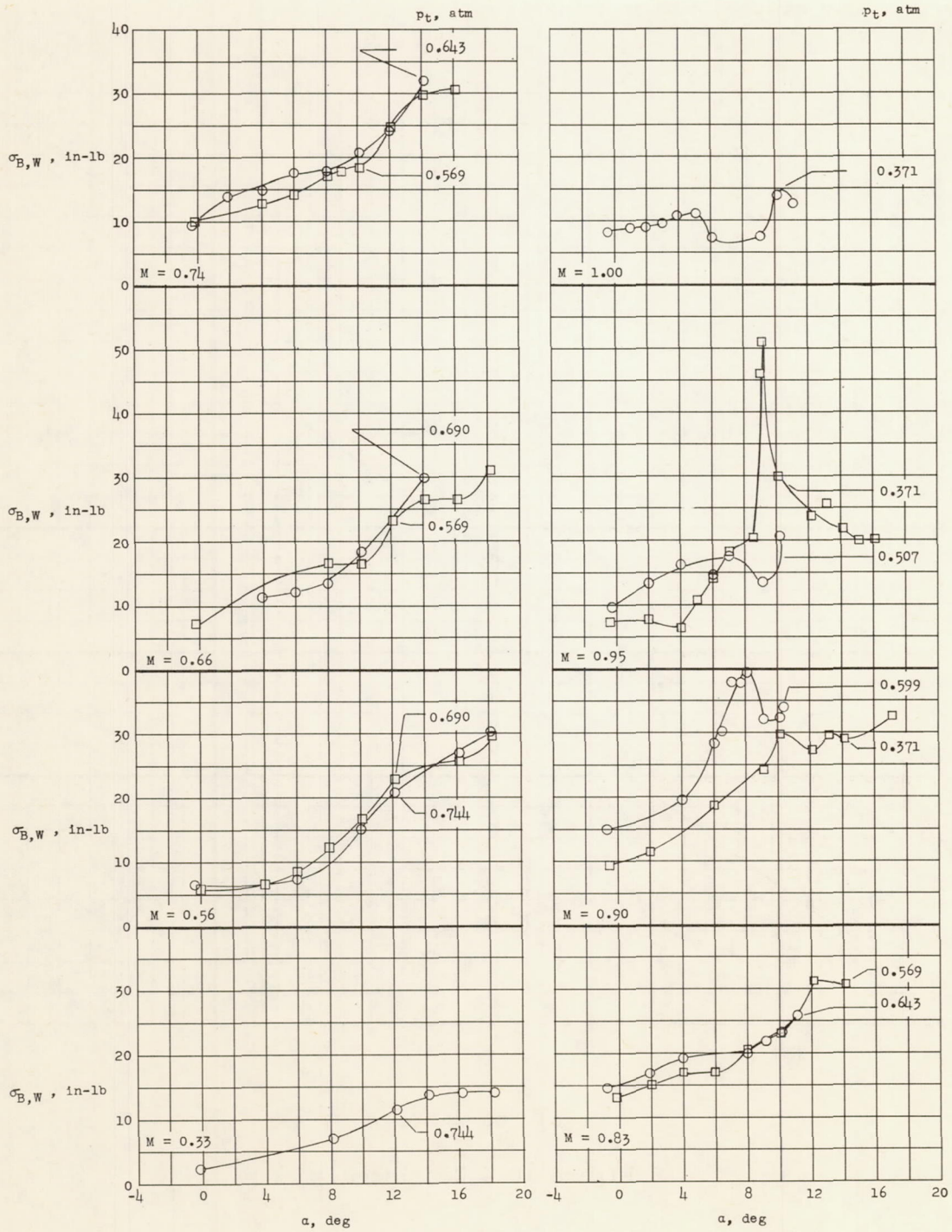

Figure 11.- Root-mean-square values of wing bending-moment fluctuations. Basic wing; $\delta_H = -6^{\circ}$.

L-1883

L-1883

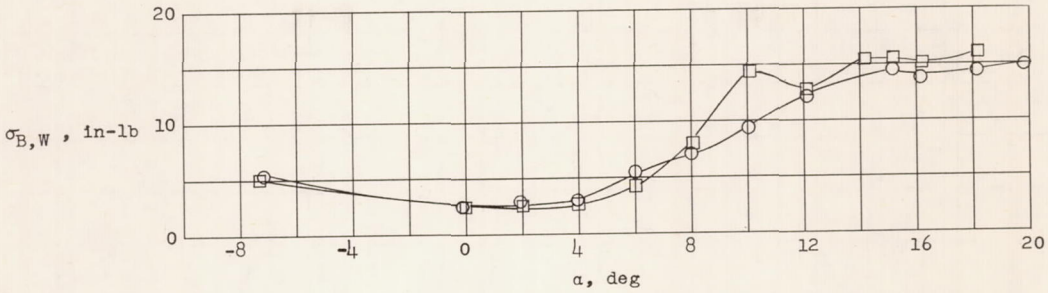

(a) M = 0.33; p_t = 0.744 atmosphere.

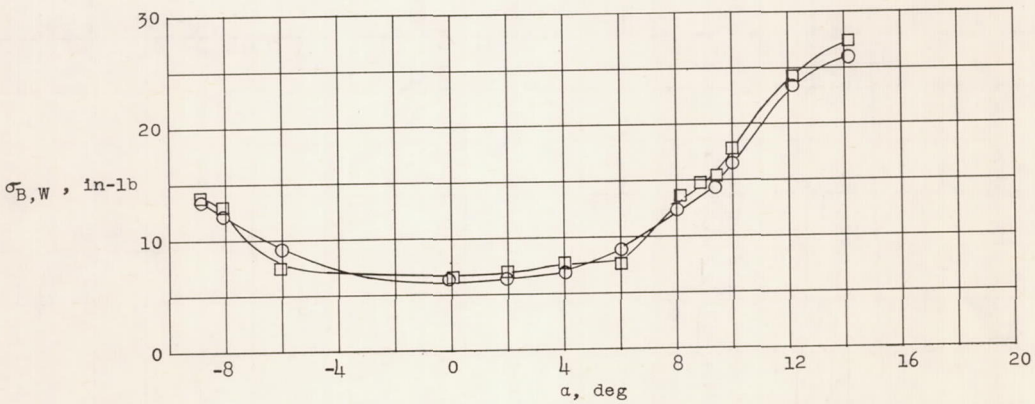

(b) M = 0.56; p_t = 0.690 atmosphere.

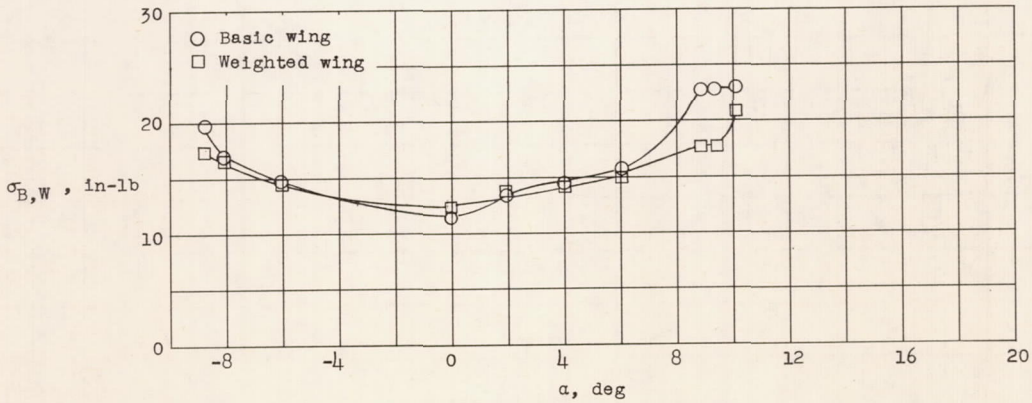

(c) M = 0.74; p_t = 0.643 atmosphere.

Figure 12.- Effect of wing mass on root-mean-square values of wing bending-moment fluctutations. $\delta_H = 0^\circ$.

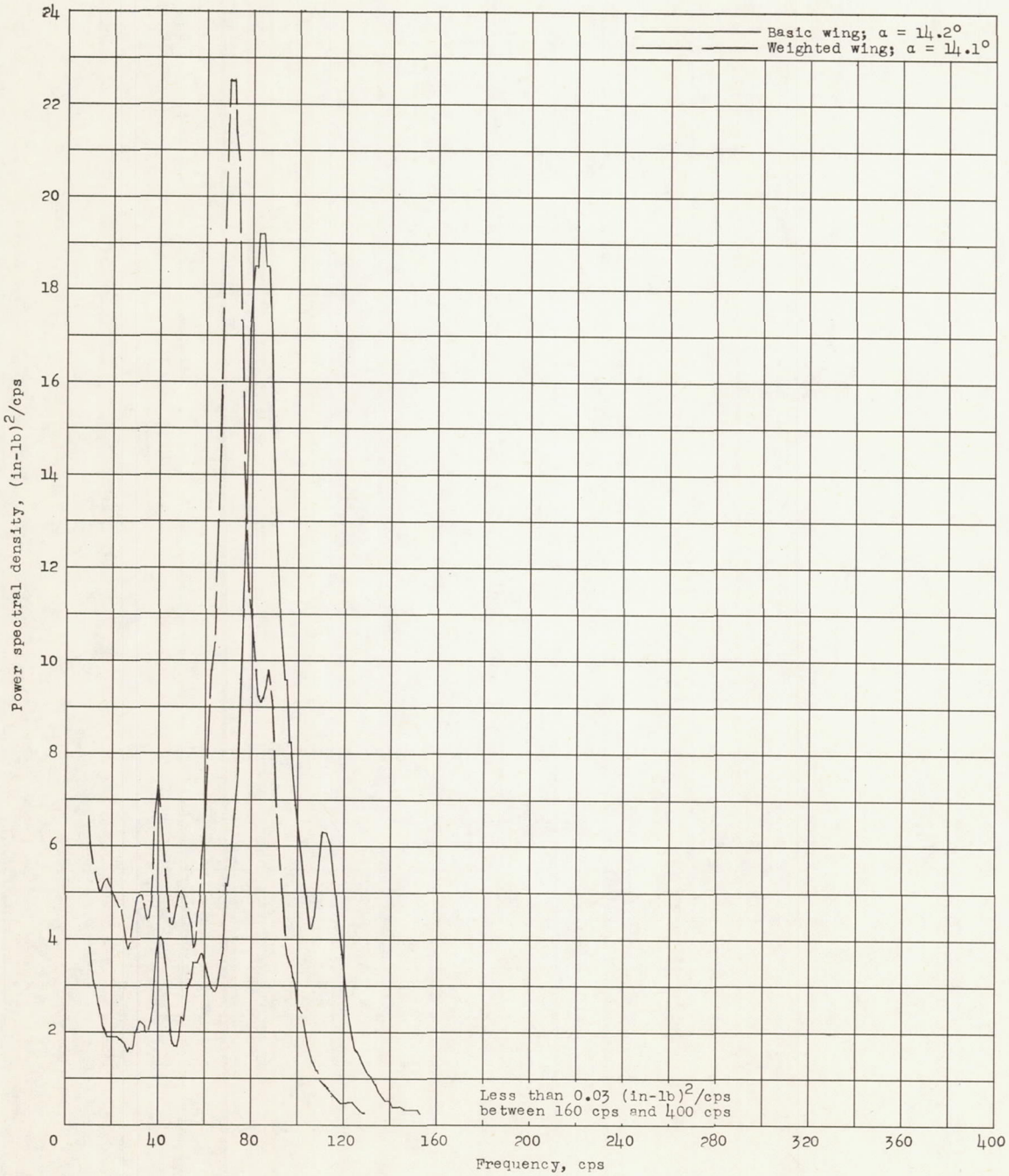

Figure 13.- Effect of wing mass on power spectral density of wing bending-moment fluctuations. $M = 0.56$; $p_t = 0.690$ atmosphere.

L-1883

L-1883

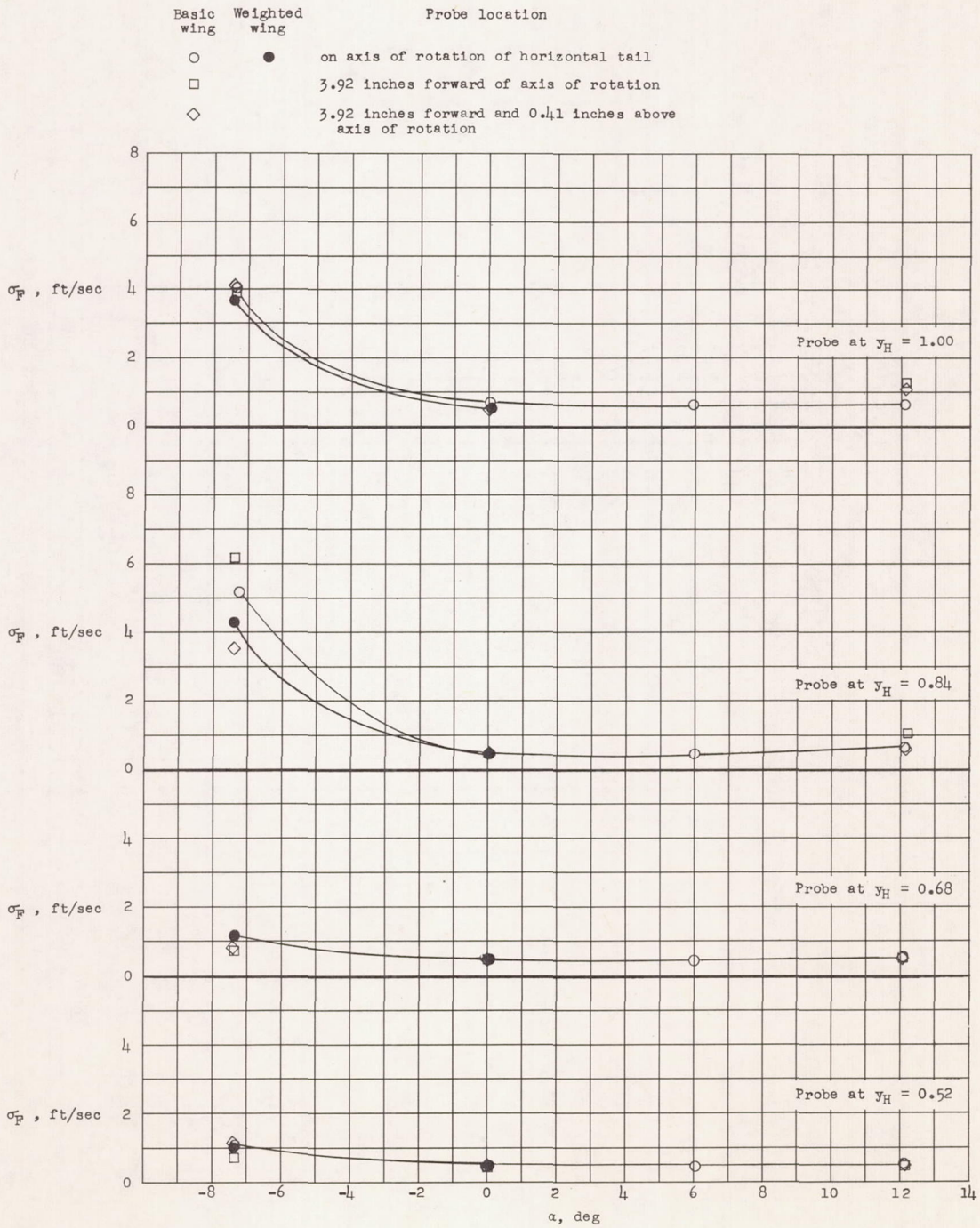

(a) M = 0.33; p_t = 0.744 atmosphere.

Figure 14.- Root-mean-square values of flow fluctuations in vicinity of horizontal tail as function of angle of attack.

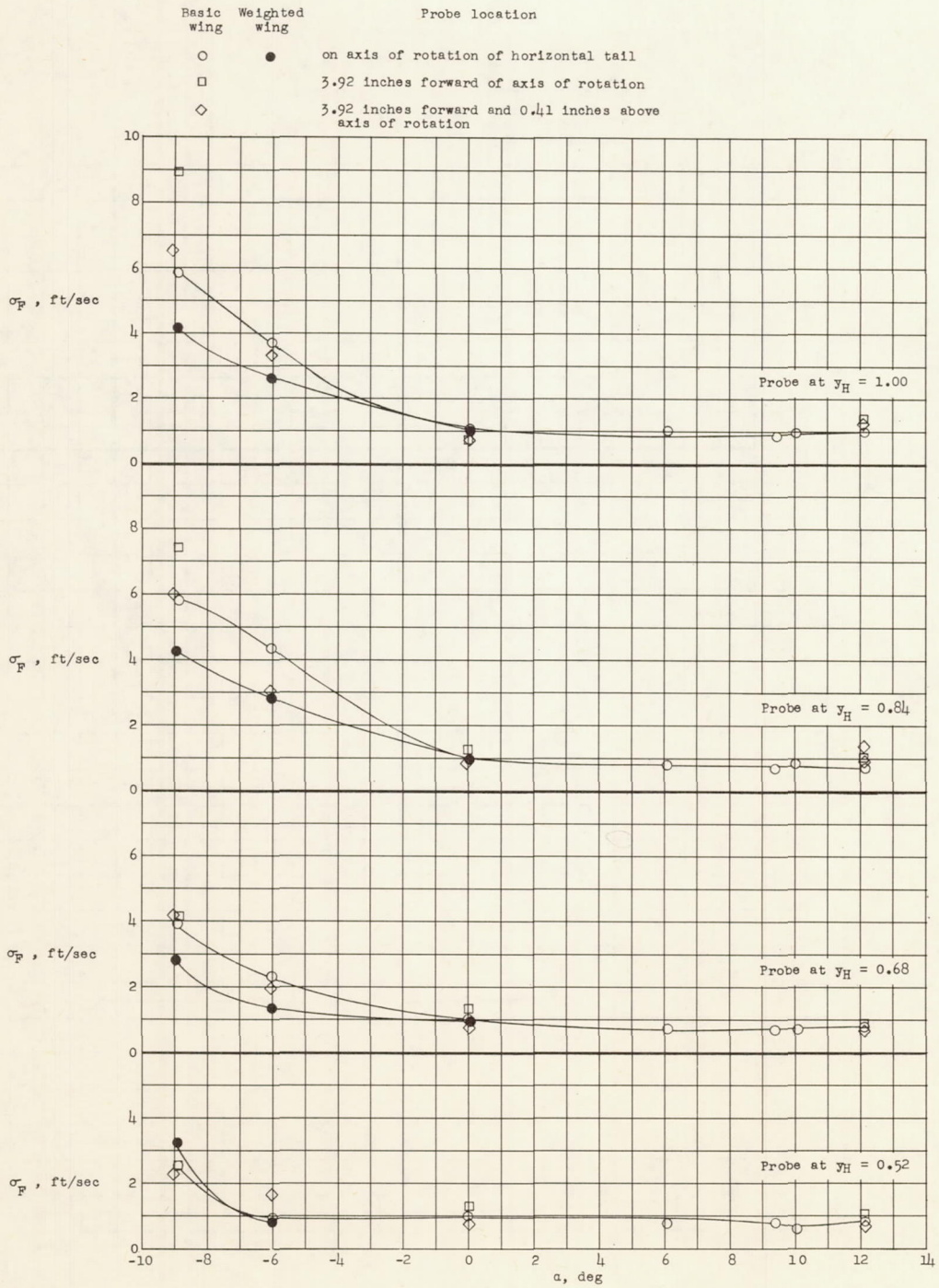

(b) M = 0.56; p_t = 0.690 atmosphere.

Figure 14.- Continued.

L-1883

L-1883

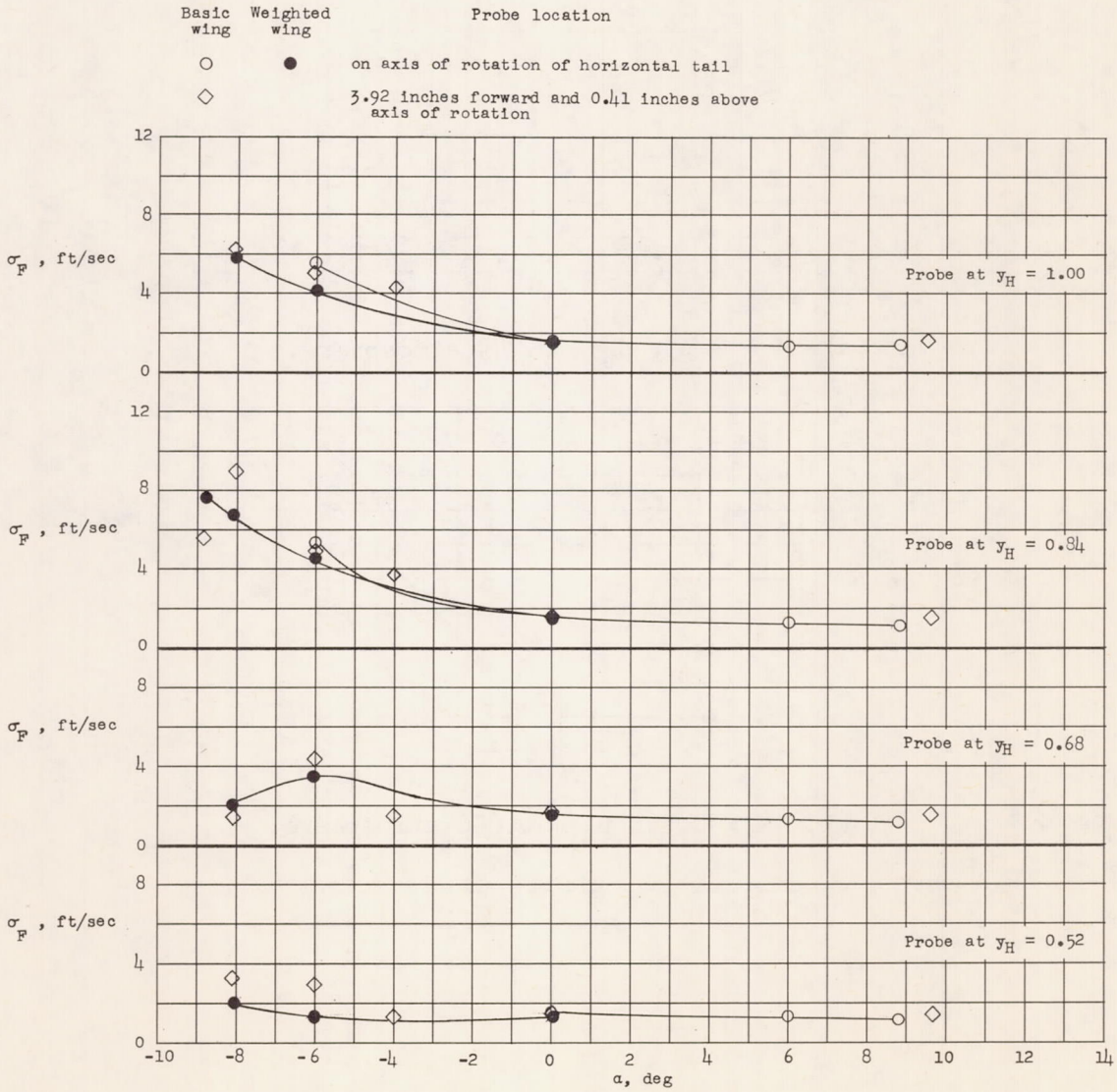

(c) M = 0.74; p_t = 0.643 atmosphere.

Figure 14.- Concluded.

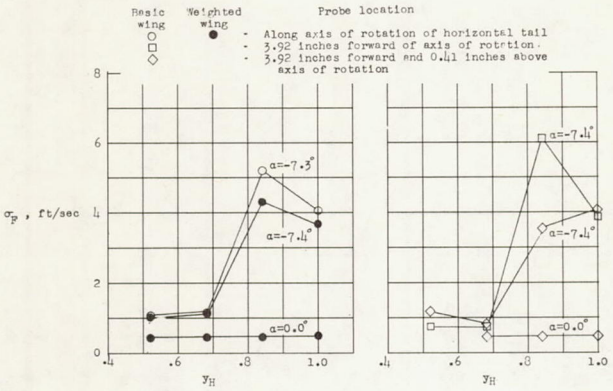

(a) M = 0.33; p_t = 0.744 atmosphere.

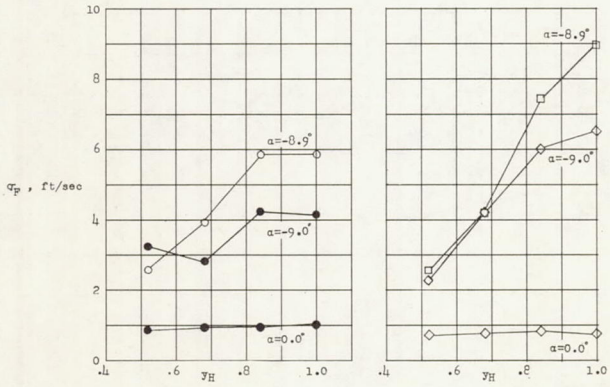

(b) M = 0.56; p_t = 0.690 atmosphere.

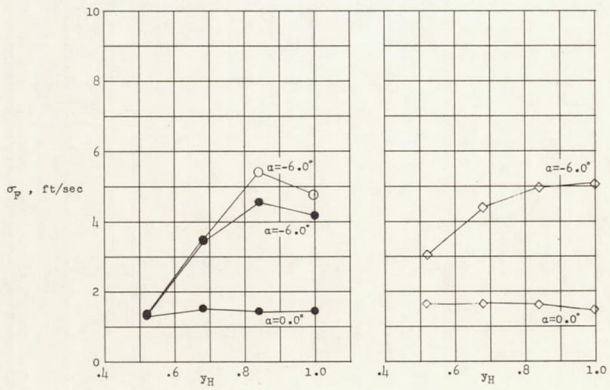

(c) M = 0.74; p_t = 0.643 atmosphere.

Figure 15.- Root-mean-square values of flow fluctuations in vicinity of horizontal tail as function of spanwise location.

L-1883

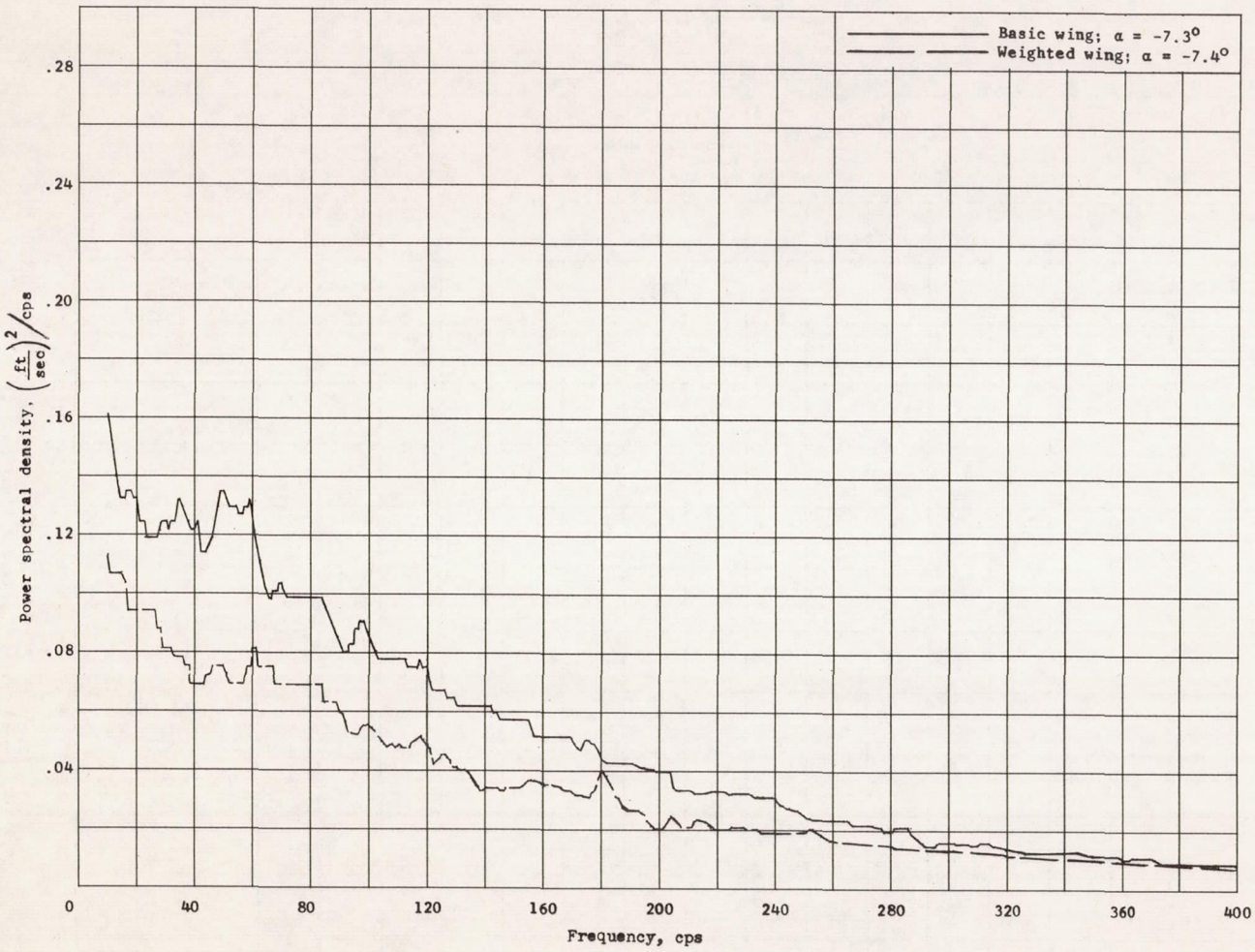

(a) M = 0.33; p_t = 0.744 atmosphere.

Figure 16.- Effect of wing mass on power spectral density of flow fluctuations in vicinity of horizontal tail. Hot wire along axis of rotation of horizontal tail at 0.84 span of the horizontal tail.

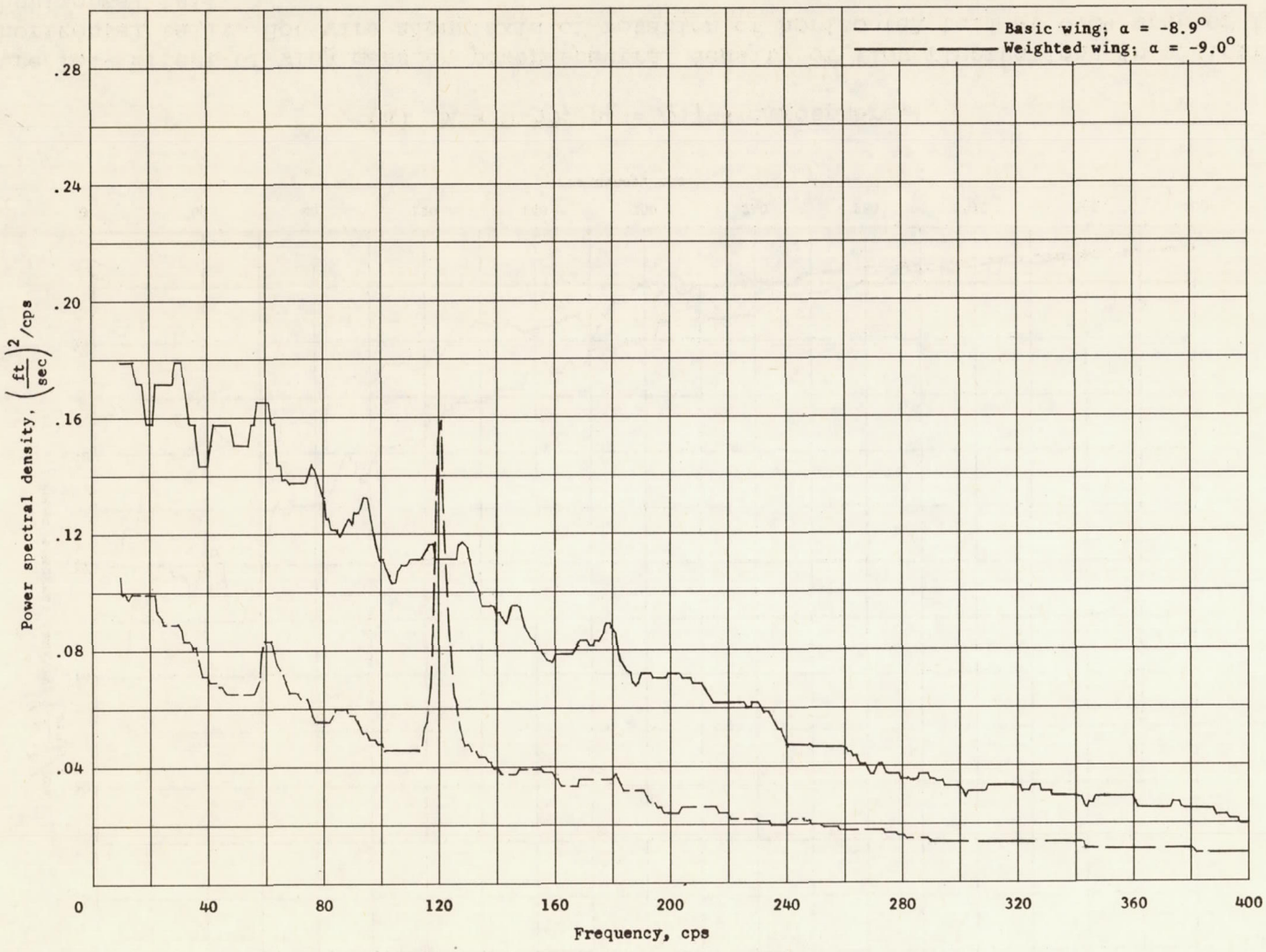

(b) M = 0.56; p_t = 0.690 atmosphere.

Figure 16.- Continued.

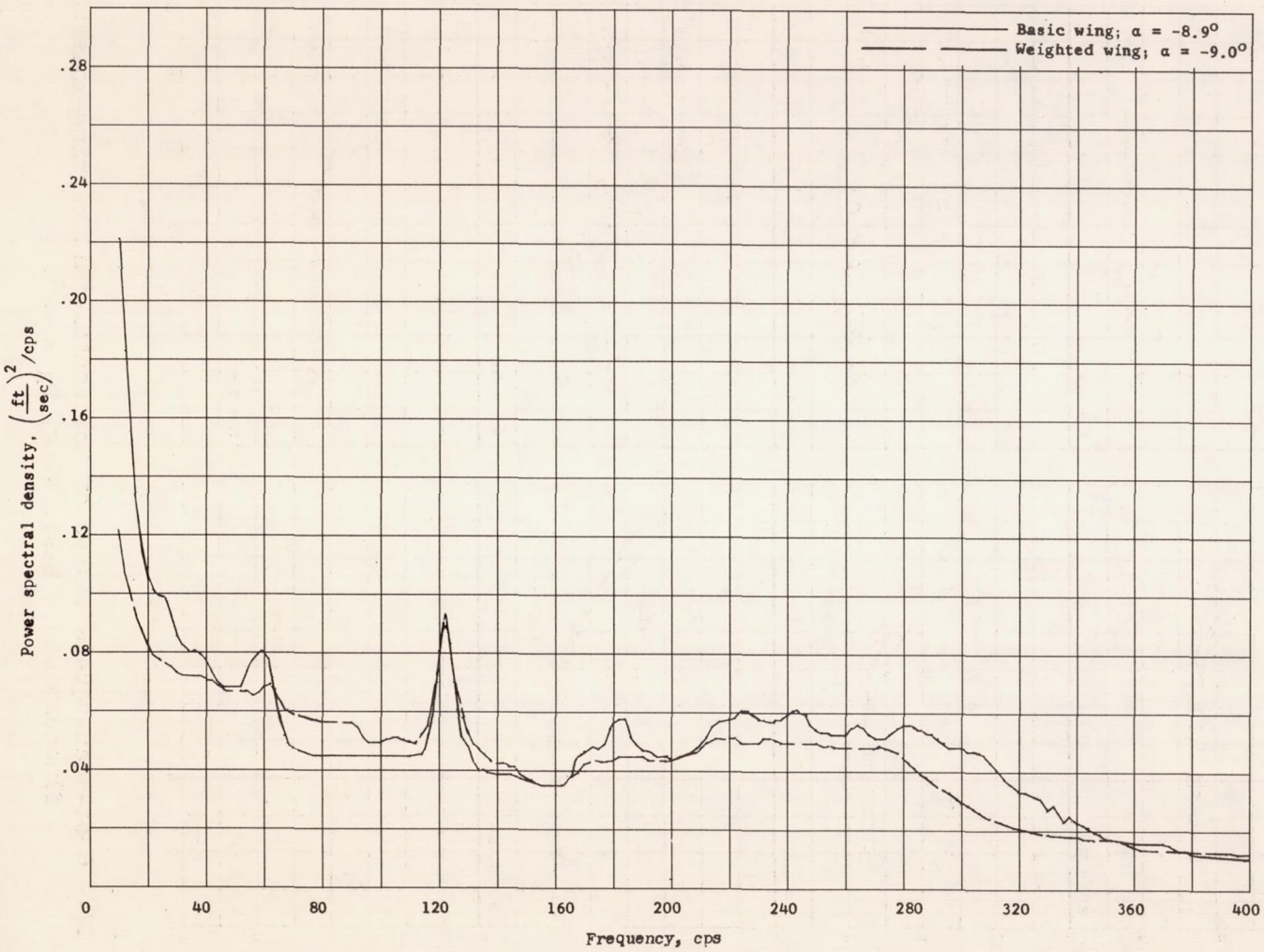

(c) M = 0.74; p_t = 0.643 atmosphere.

Figure 16.- Concluded.

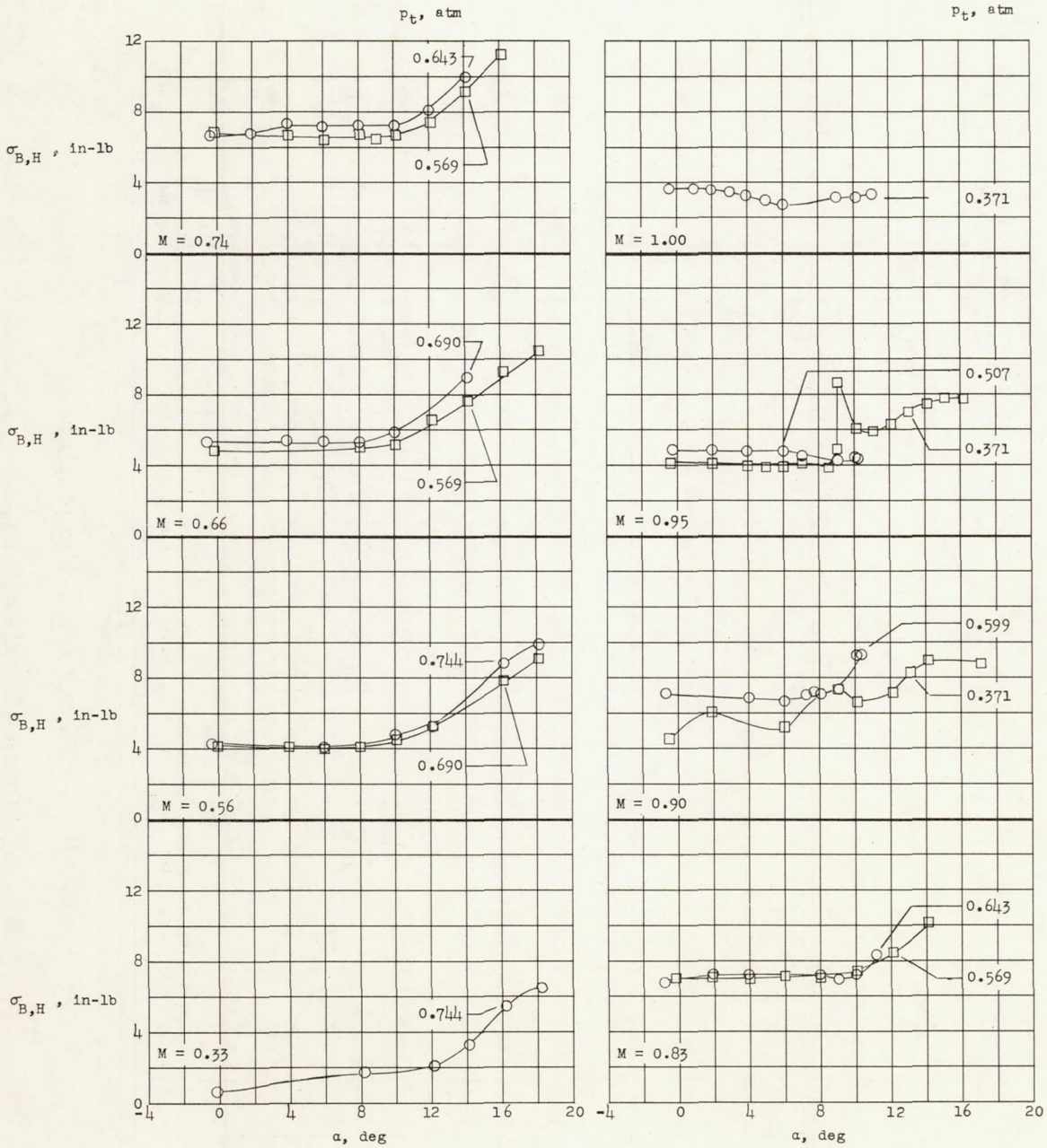

Figure 17.- Root-mean-square values of horizontal-tail bending-moment fluctuations. Basic wing; $\delta_H = -6^\circ$.

L-1883

L-1883

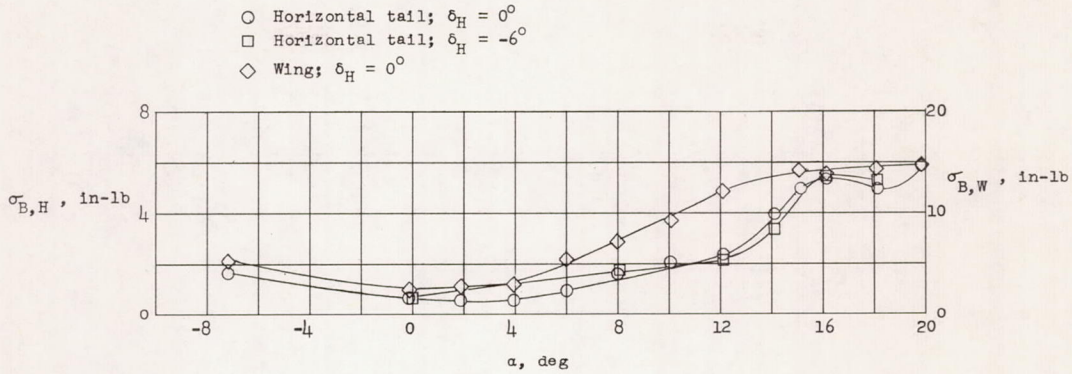

(a) M = 0.33; p_t = 0.744 atmosphere.

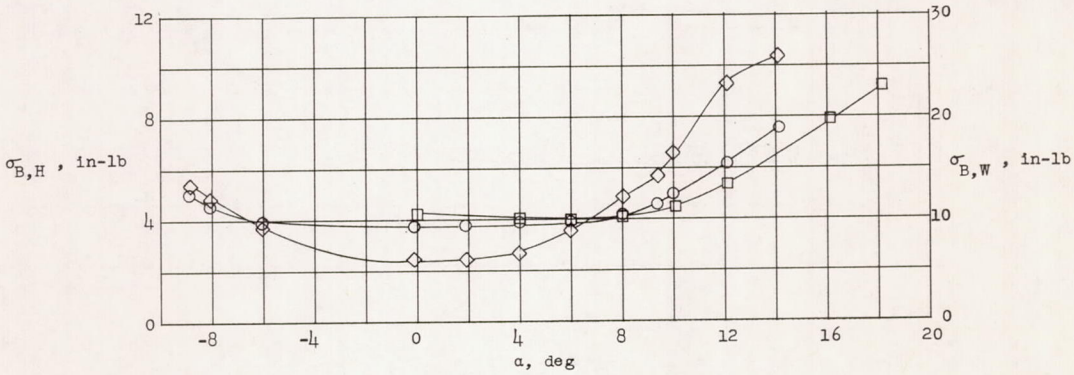

(b) M = 0.56; p_t = 0.690 atmosphere.

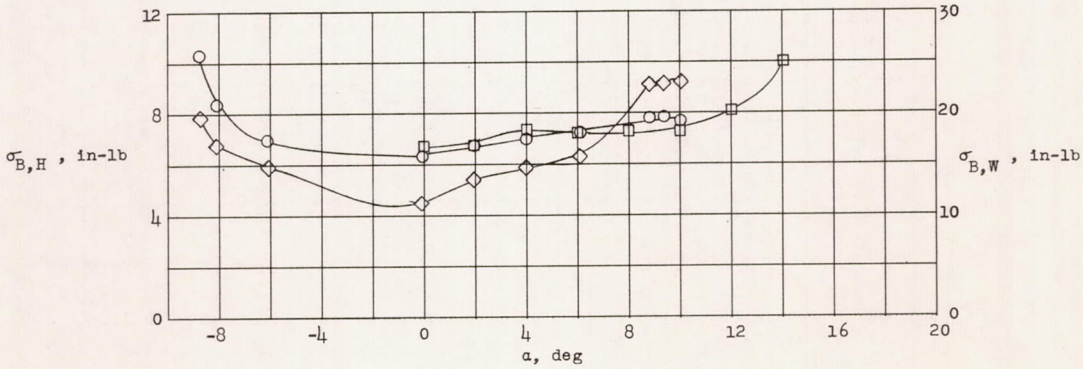

(c) M = 0.74; p_t = 0.643 atmosphere.

Figure 18.- Effect of horizontal-tail incidence on root-mean-square values of horizontal-tail bending-moment fluctuations and comparison of horizontal-tail and wing bending-moment fluctuations. Basic wing.

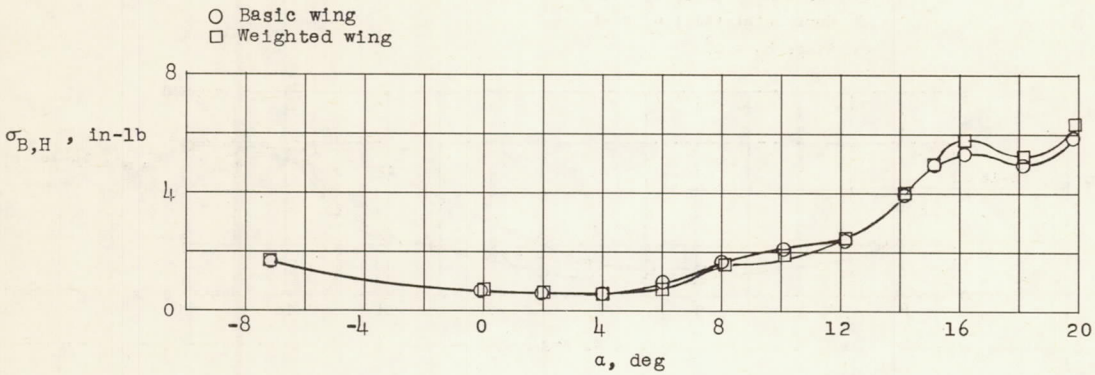

(a) M = 0.33; p_t = 0.744 atmosphere.

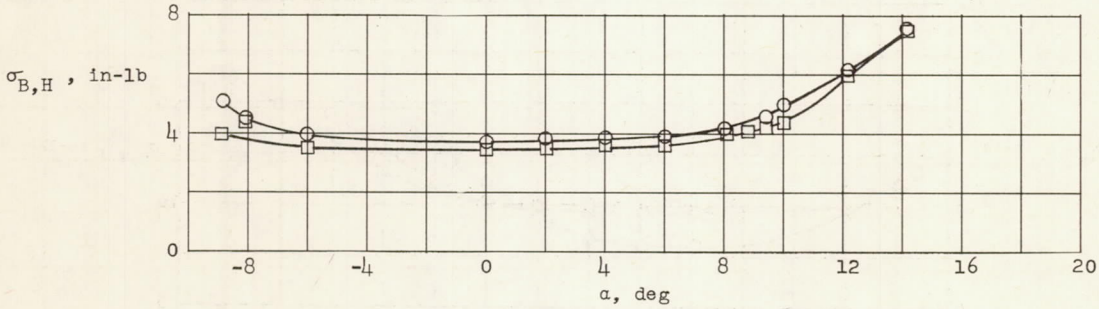

(b) M = 0.56; p_t = 0.690 atmosphere.

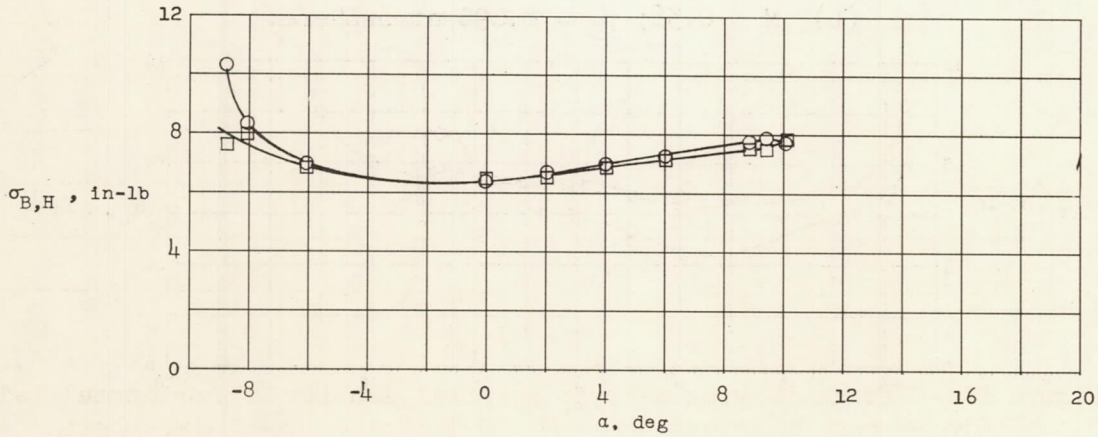

(c) M = 0.74; p_t = 0.643 atmosphere.

Figure 19.- Effect of wing mass on root-mean-square values of horizontal-tail bending-moment fluctuations. $\delta_H = 0^{\circ}$.

L-1883

L-1883

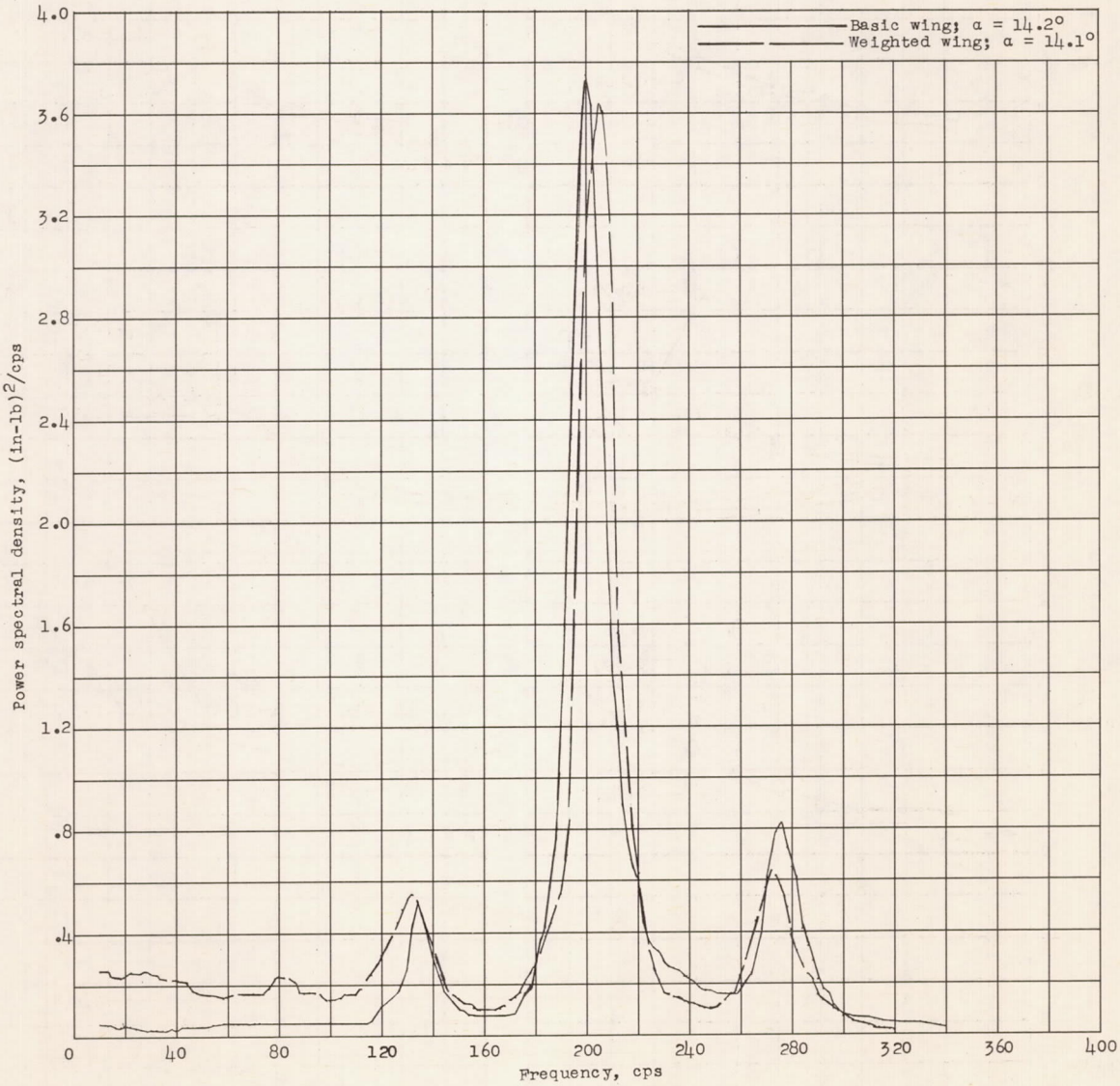

Figure 20.- Effect of wing mass on spectral density of horizontal-tail bending-moment fluctuations. $M = 0.56$; $p_t = 0.690$ atmosphere.

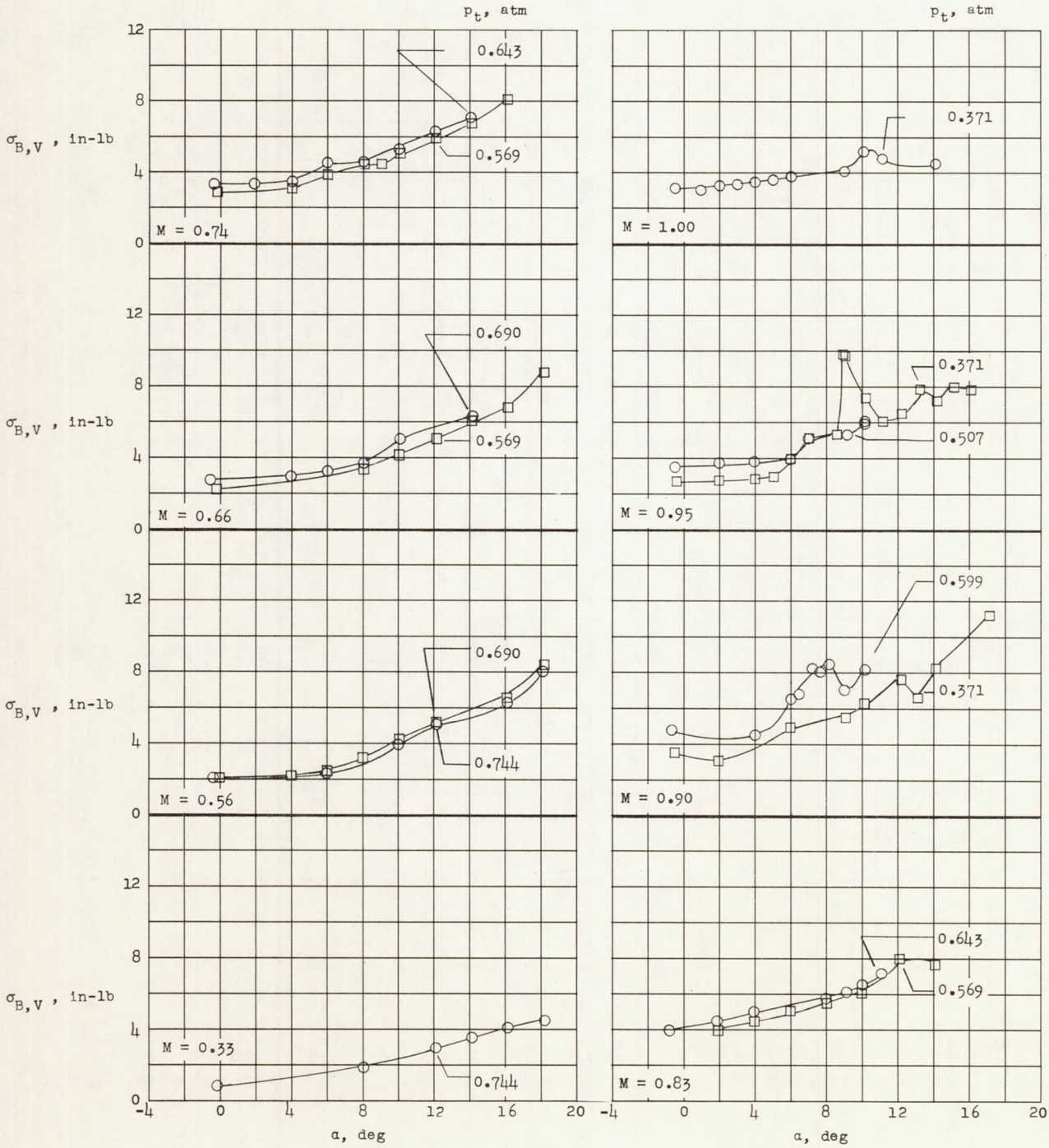

Figure 21.- Root-mean-square values of vertical-tail bending-moment fluctuations. Basic wing; $\delta_H = -6^{\circ}$.

L-1883

L-1883

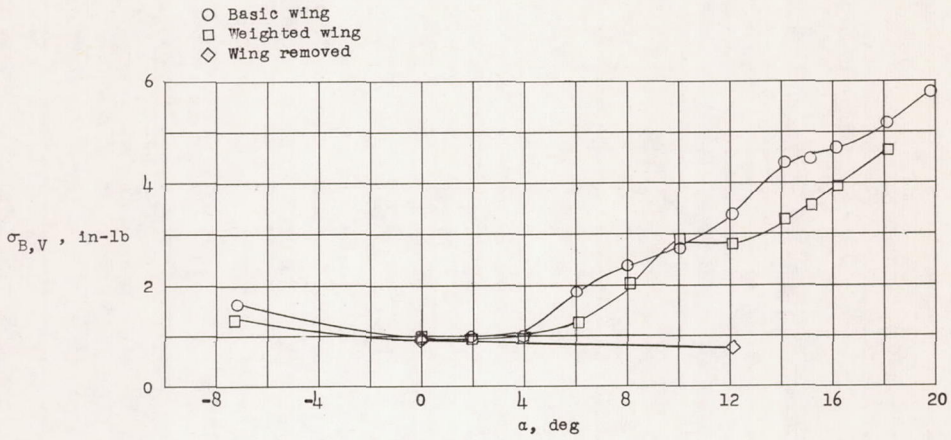

(a) M = 0.33; p_t = 0.744 atmosphere.

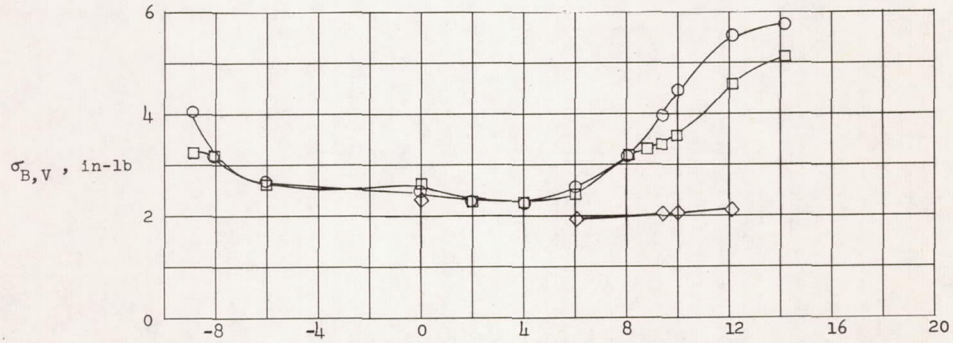

(b) M = 0.56; p_t = 0.690 atmosphere.

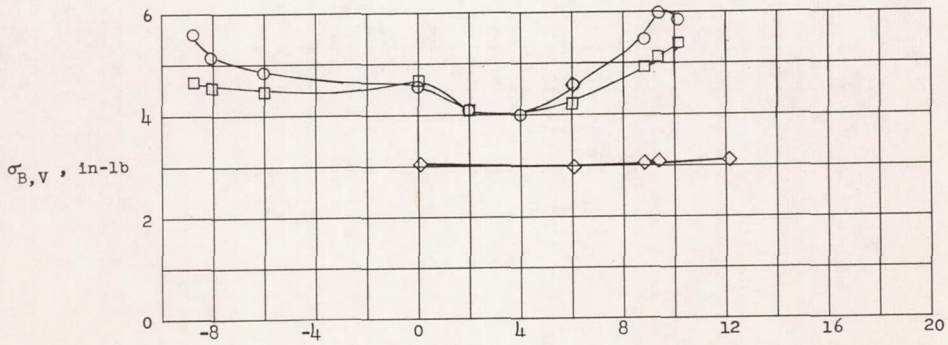

(c) M = 0.74; p_t = 0.643 atmosphere.

Figure 22.- Effect of wing configuration on root-mean-square values of vertical-tail bending-moment fluctuations. $\delta_H = 0^{\circ}$.

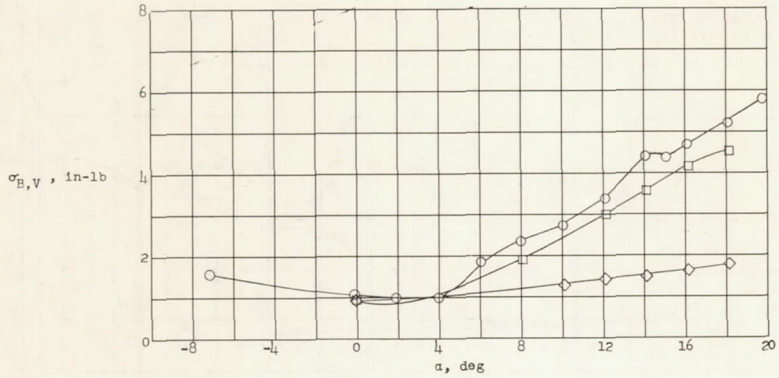

(a) M = 0.33; p_t = 0.744 atmosphere.

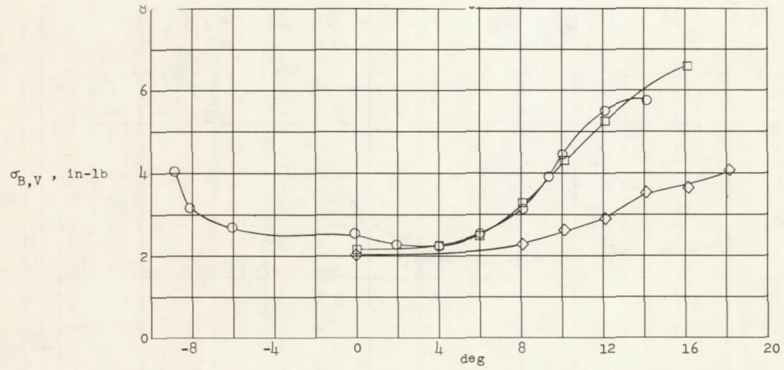

(b) M = 0.56; p_t = 0.690 atmosphere.

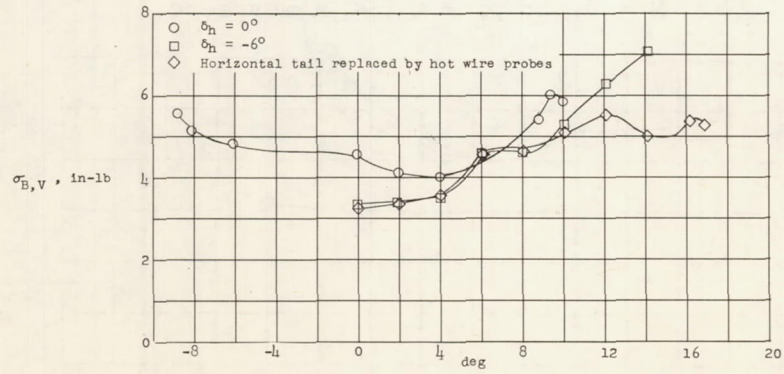

(c) M = 0.74; p_t = 0.643 atmosphere.

Figure 23.- Effect of horizontal-tail configuration on root-mean-square values of vertical-tail bending-moment fluctuations. Basic wings.

L-1883

L-1883

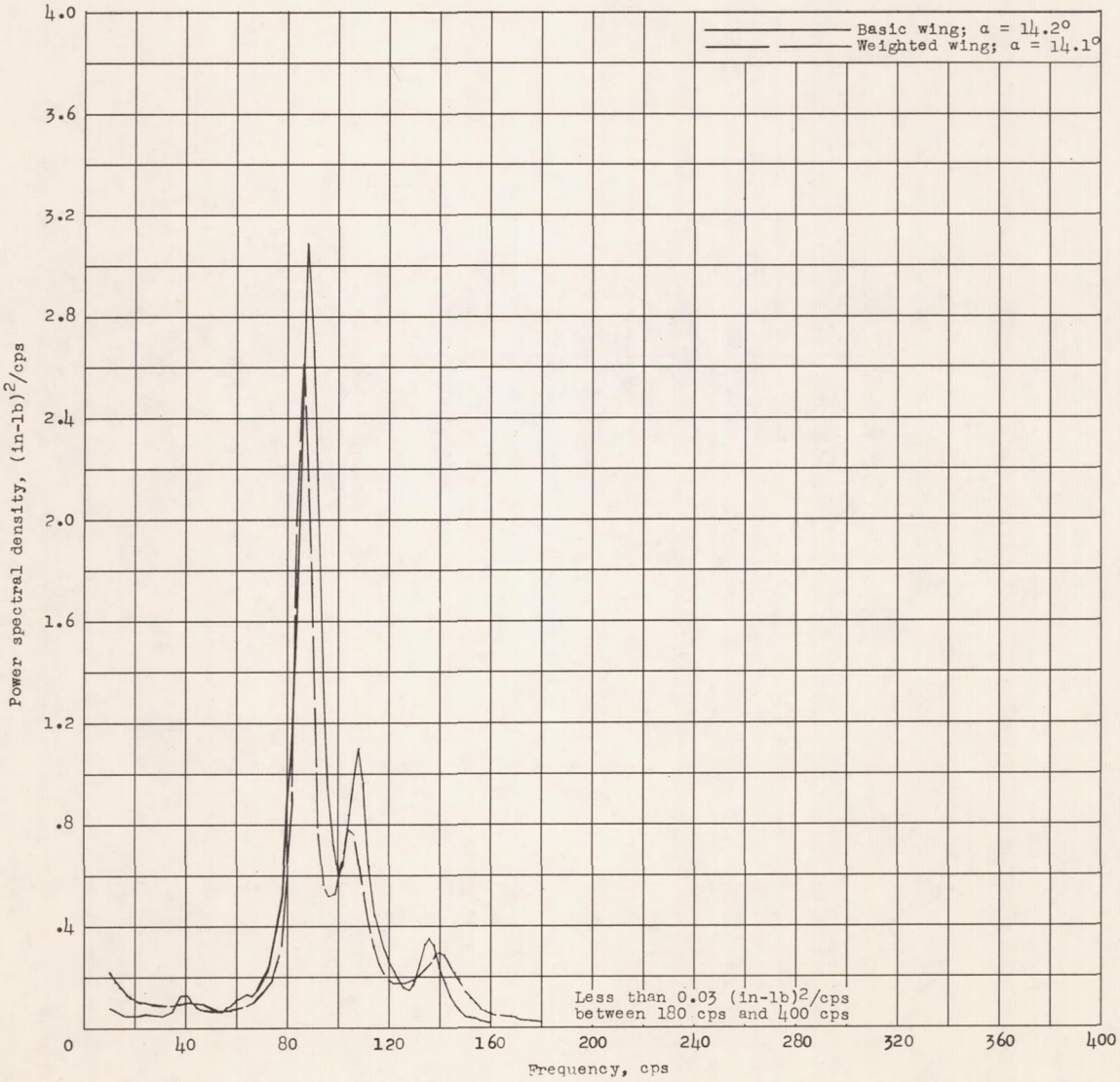

Figure 24.- Effect of wing mass on power spectral density of vertical-tail bending-moment fluctuations. $M = 0.56$; $p_t = 0.690$ atmosphere.